Plasma response to rotating resonant magnetic perturbations with a locked mode in the J-TEXT tokamak

Nengchao Wang[1], Bo Rao[1,*], Qiming Hu[2], Yonghua Ding[1], Zhipeng Chen[1], Zhoujun Yang[1], Daojing Guo[1], Zhuo Huang[1], Xinke Ji[1], Da Li[1], Jianchao Li[1], Mao Li[1], Xiaoming Pan[1], Guo Xu[1], Q. Yu[3], G. Zhuang[1], Yuan Pan[1] and the J-TEXT team

[1] International Joint Research Laboratory of Magnetic Confinement Fusion and Plasma Physics, State Key Laboratory of Advanced Electromagnetic Engineering and Technology, School of Electrical and Electronic Engineering, Huazhong University of Science and Technology, Wuhan 430074, People's Republic of China

[2] Princeton Plasma Physics Laboratory, Princeton NJ 08543-0451, USA

[3] Max-Planck-Institut für Plasmaphysik, 85748 Garching, Germany

E-mail: borao@hust.edu.cn, wangnc@hust.edu.cn

Abstract

Disruption caused by locked modes (LMs) is one of the most critical issues to be solved for tokamak fusion reactors. This paper aimed to understand the plasma response to external rotating resonant magnetic perturbations (RMPs), which are applied at a few kilohertz for controlling the pre-existing LMs. In the J-TEXT tokamak, the plasma response to a rotating RMP showed a feature of travelling wave, if no tearing mode (TM) existed. With a LM, the application of a rotating RMP led to unique features of plasma responses, which could be roughly described by the formula $\delta b_\theta(\theta, t) = 2Asin(m\theta - m\theta_O)cos(2\pi f_{RRMP}t)$, where δb_θ, A, m, θ_O and f_{RRMP} are the perturbed poloidal magnetic field, the amplitude, the poloidal mode number, the poloidal location of the TM's O-point and the frequency of the rotating RMP. These features are analogous to that of a standing wave in the TM rest frame, with the nodes locating at the O-/X- points. The perturbations of electron temperature, T_e, due to plasma responses were zero or minimal inside the magnetic island or outside the magnetic island but at the same poloidal positions as the O-/X- points. Both δb_θ and the T_e perturbations increased linearly with the rotating RMP. A phenomenological model is proposed that the rotating RMP drives the phase oscillation of the TM by applying a periodical electromagnetic torque. Then the phase oscillation of TM, combined with the poloidal gradient of the plasma parameters, induces the plasma response measured experimentally. The nonlinear numerically modelling confirmed the forced phase oscillation of the TM, and qualitatively verified the amplitude and phase dependences among the plasma response, the phase oscillation of the TM and the rotating RMP, which have been predicted by the model.

* Authors to whom any correspondence should be addressed.

1. **Introduction**

The externally applied magnetic perturbation (MP) fields have been widely applied in tokamak plasmas to control the magnetohydrodynamic (MHD) instabilities [1, 2], such as tearing mode (TM) [3-7], resistive wall mode (RWM) [8, 9] and edge-localized modes (ELMs) [10, 11]. When the MP field has the same helicity as the magnetic field line of a rational surface within the last closed flux surface, the MP field and the surface are named as the resonant MP (RMP) field and the resonant surface (RS), respectively. Due to the plasma flow at the RS, the plasma response could screen the RMP field from penetrating into the region inside the RS [12-15]. In addition, the plasma also responds to the non-resonant component of MP fields, modifies the poloidal spectrum of the total MP field [16, 17] and results in the dependence of MHD control on the poloidal spectrum [18-20] of external MP fields. Hence, understanding the plasma response to the MP field is essential for the robust control of these instabilities, especially with the presence of a MHD mode. With a pre-existing external kink mode, the plasma response driven by the external MP field was observed to be independent to the external kink mode in HBT-EP [21]. The RWM could be unlocked from the resistive wall by the feedback applied MP field in the RFX-Mod device [22, 23], a reversed field pinch. With the presence of a TM at the RS, the TM reacts to the RMP field and hence contributes to additional plasma response. Experimental and theoretical studies demonstrate that the TM could be either locked [4-6, 24-26] or suppressed [4-6, 27, 28] by the RMP field.

The locked mode (LM) is a non-rotating tearing mode, formed due to the locking [4-6] of a rotating magnetic island or the penetration [12] of the error field / RMP field. A LM usually grows to a large amplitude, and leads to severe confinement degradation or even to disruptions [4]. The major disruption due to LM is an important issue for ITER, since the locking threshold of a neoclassical TM [29, 30] and the penetration threshold at the low density start-up phase [31] are low for the error field on ITER. The RMP field applies an electromagnetic (EM) torque [5] on the LM, and has been widely applied to control or avoid the LM both experimentally [32-37] and theoretically [36-38]. The RMP has been investigated to steer the LM's O-point to the deposition region of electron cyclotron current drive (ECCD), as a result the LM is completely suppressed as predicted by modelling [29] and realized in DIII-D experiments [32, 33]. In DIII-D, the avoidance of NTM locking and its associated disruption by applying RMPs regulated by a feedback system has been explored [37], and the LM was unlocked and entrained up to 125 Hz [36]. These DIII-D studies focus on the strategy for feedback control and the torque balance with applying static or low frequency (<

200 Hz) rotating RMP (RRMP) field, and have not described the evolutions of the plasma parameters around the magnetic island.

By applying a RMP field rotating at a few kilohertz, the LM has been unlocked and accelerated to the RRMP frequency, f_{RRMP}, in TEXTOR [34] and J-TEXT [35]. In TEXTOR, the secondary structures were observed from the soft x-ray (SXR) and electron cyclotron emission (ECE) measurements around the large locked m/n = 2/1 TM , where m and n are the poloidal and toroidal mode number, respectively. In J-TEXT, the unlocking threshold of RRMP has been studied as a function of f_{RRMP} and the unlocking process has been modelled nonlinearly based on reduced MHD equations. The detailed plasma responses during the LM stage are important for understanding the unlocking process and predicting its threshold, but they are not fully understood.

Motivated by these results, we carried out a systematic study on the plasma response to a RRMP field in the presence of a LM in J-TEXT both experimentally and numerically. In the experiments, the plasma responses, measured by the perturbations of poloidal magnetic field and electron temperature, showed a standing wave like feature in the TM rest frame and the response was minimal poloidally at the O-/X- points of the island. These features could be described by a phenomenological model that the RRMP drives the phase oscillation of the TM by applying a periodical EM torque and that the phase oscillation of TM, combined with the poloidal gradient of plasma parameters, induces the plasma response measured experimentally. The nonlinear numerical modeling based on reduced MHD equations reproduces the experimental results and the model predictions qualitatively, hence provides a further validation of the present theory. The sections of this paper are organized as follows. Section II describes the RMP systems and the diagnostics in J-TEXT. Section III shows the experimental results of the plasma response with and without a locked mode. A phenomenological model is proposed in Section IV, while the non-linear numerical results are introduced in Section V. Finally, Section VI gives conclusions and discussions.

2. Experimental set-up

The plasma in the J-TEXT tokamak has a circular cross-section with major radius R = 105 cm and minor radius a = 25 - 29 cm adjusted by a movable limiter [39]. In this paper, the plasmas were operated with a = 26 cm, the toroidal field B_t = 1.58 T, the plasma current I_p = 160 kA, and the edge safety factor q_a = 3.15. A set of out-vessel RMP coils [40] was used to apply a 2/1 static RMP (SRMP) field to lock the rotating 2/1 TM, while the RRMP fields were also applied to study the plasma

response to RMP field by feeding AC currents into the in-vessel RMP coils [40, 41], also named the dynamic-RMP (DRMP) or RRMP coils. In the J-TEXT Ohmic plasmas, the 2/1 tearing modes are observed to rotate only in the electron diamagnetic drift direction. This corresponds to the counter-I_p direction if mapped to the toroidal direction. Hence, the counter-I_p direction is defined as the positive direction for both 2/1 TM and the RRMP field.

The RRMP coils consist of 12 saddle coils (3 rows × 4 columns × 1 turn), as shown in Fig. 1. Two power supplies [42] were used to feed AC currents with the waveform of $I_c = I\times\sin(2\pi f_{AC}t + \delta_i)$ into the RRMP coils, where I the amplitude with a maximum of 6 kA, f_{AC} the frequency within the range of 1 ~ 6 kHz, and δ_i the phase as listed and marked by the different colors in Fig. 1. δ_i of 4 RRMP coils in each row were selected to increase (respectively decrease) by 90^o successively from left to right, hence a RMP field with toroidal mode number $n = 1$ and rigidly rotating in the counter-I_p (co-I_p respectively) direction was generated at the frequency of $f_{RRMP} = f_{AC}$. δ_i of the 3 RRMP coils in each column were selected to increase by 180^o successively from top to bottom to guarantee that the $n = 1$ RMP field had a dominant poloidal mode number of $m = 2$.

A coordinate ξ is defined by $\xi = m\theta + n\varphi$ as indicated by the arrow in the lower left in Fig. 1, where θ and φ are the poloidal and toroidal angles respectively. Using the large tokamak aspect ratio approximation for simplification, the field line is straight in φ-θ panel and ξ is constant at a fixed field line. The field lines at the $q = 2/1$ RS with two different ξ values are shown by the dashed and solid gray lines in Fig. 1.

The distribution of the $m/n = 2/1$ RMP field can then be expressed as $b_r^{2/1}\times\cos(\xi + \delta^{2/1})$ for the SRMP, the RRMP and the error field, where $b_r^{2/1}$ and $\delta^{2/1}$ represent the amplitude and phase of 2/1 RMP field. $\delta^{2/1}$ is constant and $b_r^{2/1} = 0.55$ Gauss/kA at $r = a$, for the SRMP applied in this paper [40]. The RRMP coils can induce eddy currents in the wall and the corresponding attenuation effect saturates above 1 kHz. $b_r^{2/1}$, calculated at $r = a$, is 0.45 ~ 0.55 Gauss/kA for the RRMP field in the frequency range of 1 ~ 6 kHz [40, 43]. For the RRMP, $\delta^{2/1} = 2\pi f_{RRMP}t + \delta_0^{2/1}$, where $\delta_0^{2/1}$ is the phase of RRMP at $t = 0$. The RRMP was applied in the counter-I_p direction, which corresponds to the electron diamagnetic drift direction in this paper.

Three sets of diagnostics are used to measure the TM and the plasma responses to RRMP fields, as shown in Fig. 1. Two pairs of locked mode detectors (LMDs) [44], measuring the radial magnetic field, b_r, were installed at the low field side mid-plane ($\theta_{LMD} = 0^o$) and outside the stainless-steel vacuum vessel with 16 mm thickness. Since the high frequency (> 500 Hz) component of b_r is

completely screened, only the static or quasi-static component of b_r from the plasma can be measured. By fitting the b_r signals from LMDs against their toroidal locations using a sine function with n = 1, the amplitude of n = 1 component of b_r, $b_r^{n=1}$, and its phase at the peak, $\varphi^{n=1}$, could be measured. When there is a large 2/1 LM, the LM is the main source of $b_r^{n=1}$. Under the present helicity of the field line, the O-point of the LM is located at $\xi_O^{2/1} = \xi^{n=1} + 90^o = \varphi^{n=1} + 90^o$.

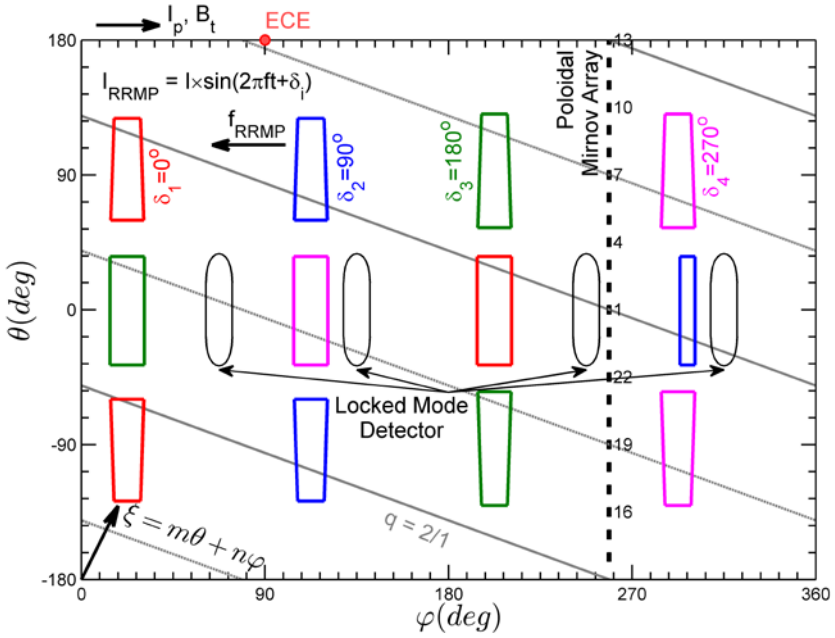

Fig. 1 The toroidal arrangement of the RRMP coils (thick lines), the poloidal Mirnov array, the locked mode detector and the ECE in J-TEXT. The field lines at the q = 2 resonant surface are also plotted with a straight field line assumption. The phases of AC currents in RRMP coils are marked for the top row and indicated by the color for the rest. A coordinate is defined by $\xi = m\theta + n\varphi$, where m = 2 and n = 1 is used.

A poloidal Mirnov array, located at φ_{Mir} = 259°, measures db_θ/dt at the whole poloidal cross-section. The high frequency component of the perturbed poloidal magnetic field, δb_θ, due to the rotating TM or the plasma responses to RRMP fields is obtained by integrating db_θ/dt numerically and applying a high pass filter. Besides, an 8-channel heterodyne electron cyclotron emission (ECE) radiometer [45] was used to measure the ECE radiation. With relative calibration, it provides the radial distribution of electron temperature (T_e) covering the 2/1 RS at the in-board mid-plane (θ_{ECE} = 180°) with the toroidal phase φ_{ECE} = 90°. T_e or T_e perturbation are in arbitrary units for the data shown in this paper.

The plasma responses to RRMP fields are then quantitatively reflected by the magnetic perturbations and electron temperature perturbations measured at f_{RRMP} and $2f_{RRMP}$, i.e. $\delta b_\theta(f_{RRMP})$, $\delta b_\theta(2f_{RRMP})$ and $\delta T_e(f_{RRMP})$. The time evolutions of their amplitudes are obtained by fitting δb_θ and T_e using the formula, $a = a^{ave} + \delta a(f)\times\sin[2\pi ft + \phi(f)] + \delta a(2f)\times\sin[2\pi\times 2ft + \phi(2f)]$, where a represents b_θ or T_e and f equals f_{RRMP}, for a sets of time durations of $2/f_{RRMP}$.

3. Experimental results

The applied RRMP field could be effectively shielded by the rotation of plasma at the RS [12]. The degree of the screening effect is mainly affected by the slip frequency between the MHD mode and the RMP field, $f_s = f_{MHD} - f_{RMP}$, and the resistivity at the resonant surface. We start in Section 3.1 by describing a simple experiment, where the RRMP field was applied to a plasma without large saturated TMs and $f_s > 0$, and show that the plasma response is travelling wave and due to the screening effect at the resonant surface.

The plasma response to RRMP is more complicated if a quasi-static TM exists as described in Section 3.2, and it is shown that the corresponding magnetic perturbation has a *standing wave like* structure while the temperature perturbation is strongly related to the structure of the magnetic island. The above features also exist if the TM is locked as shown in Section 3.3, and the amplitude of the response depends linearly on the RRMP amplitude. The plasma response to RRMP is compared and summarized for the cases with LMs and without TMs in Section 3.4.

3.1. Plasma response to RRMP in the tearing-stable plasma

Fig. 2 displays the discharge #1032189 as an example of the plasma response to a 4 kHz RRMP without large saturated TMs. Before the application of RRMP, there existed small magnetic oscillations (SMOs), which have been observed in the plasmas accompanying regular sawtooth crashes in J-TEXT [46] and recently reported in EAST [47]. The SMOs appeared as the structures at the frequency of 7 ~ 8 kHz in the wavelet power spectrum of the Mirnov signal as shown in Fig. 2(*b*). And they had an amplitude of around 0.5 Gauss and a dominant mode number of $m/n = 2/1$ as shown in Fig. 2(*c*) (also described previously in Ref. [46]). This indicates that the SMOs originated from the $q = 2/1$ surface and that $f_{MHD} \approx 8$ kHz at the 2/1 RS. They might be small/micro tearing modes or small kink modes, since their amplitudes are much smaller than those of typical large saturated TMs, 20 ~ 40 Gauss. A higher spatial resolution of the ECE measurement, e.g. the ECE-Imaging, is needed in J-TEXT to identify whether the SMOs are tearing modes or not. Since the SMOs are quite small, we refer to this status as *tearing-stable* for a comparison to the *tearing-unstable* status when a large saturated TM exists.

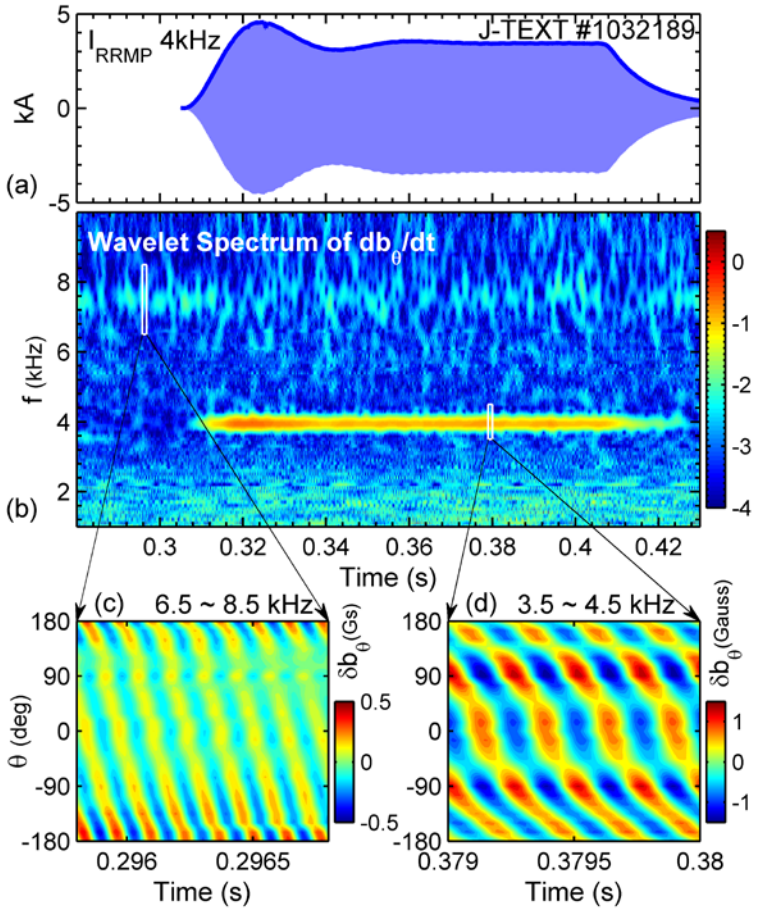

Fig. 2 Plasma response to RRMP in a tearing-stable discharge (#1032189): (*a*) the RRMP coil currents, (*b*) the wavelet power spectrum of Mirnov signal measured at $\theta = 0^{o}$. The third row shows δb_θ as a function of time and poloidal angle for (*c*) the SMO before the RRMP was applied and (*d*) the plasma response during the flattop of RRMP. δb_θ was obtained with a band-pass filter in the frequency ranges of (*c*) 6.5 - 8.5 kHz and (*d*) 3.5 - 4.5 kHz.

Once the RRMP was applied at 0.308 s (Fig. 2(*a*)), the distinct plasma responses at f_{RRMP} = 4 kHz could be observed (Fig. 2(*b*)). The evolution of the magnetic perturbations due to plasma response at various poloidal locations is shown in detail by the contour of δb_θ (within 3.5 – 4.5 kHz by using a band-pass filter) in Fig. 2(*d*). The amplitude of the magnetic perturbations due to plasma response, $\delta b_\theta(f_{RRMP})$, was larger than that due to SMOs, but still smaller than 2.5 Gauss with maximal I_{RRMP}. The measured magnetic perturbations could be observed to propagate in the negative poloidal direction by tracing the peak trajectory in Fig. 2(*d*) in time. It corresponds to the electron diamagnetic drift direction, if it is mapped to the perpendicular direction of the field line (shown in Fig. 1). Hence the measured plasma response propagated in the same direction as the RRMP field.

At each time slice in Fig. 2(*d*), there were three peaks and dips in the poloidal distribution of δb_θ, which indicates that there was a large m = 3 component of the plasma response. In addition, the amplitudes of magnetic perturbations were not constant poloidally, and the poloidal phase velocity of the peak of magnetic perturbations wasn't constant, neither. These non-uniform features might be due to the existence of an m = 2 component of the plasma response. According to the toroidal Mirnov array, the toroidal mode number was n = 1. It is noted that $\delta b_\theta(f_{RRMP})$, below 2.5 Gauss, was more than one order smaller than that due to the excitation of a 2/1 or 3/1 island when the RRMP field

penetrated, as described previously in J-TEXT [48]. And no observable change of the toroidal rotation of Carbon impurity (C^{4+}) was observed after the RRMP applied. Hence in this paper, the plasma response to RRMP in the tearing-stable plasma, which has a travelling wave feature, was not due to the excitation of a rotating 3/1 or 2/1 island during the RRMP penetration, but was due to the screening effect at q = 3/1 and 2/1 rational surface where the slip frequency f_s was not 0.

3.2. Plasma response to RRMP with a quasi-static TM

The plasma response to RRMP with a quasi-static TM has been observed in discharge 1032071, as shown in Fig. 3. In this discharge, the 2/1 TM, originally rotating at 3.2 kHz, was accelerated to 6 kHz at 0.26 s due to the application of a 6 kHz RRMP [24, 43]. Fig. 3 (*c*) displays the wavelet power spectrum of Mirnov signal indicating the rotating TMs and the plasma response at f_{RRMP} = 6 kHz. Due to some reasons which remain to be investigated, the TM unlocked from the 6 kHz RRMP at 0.3 s. Then the TM slowed down as indicated by the decrease of f_{TM} (Fig. 3 (*c*)) from 0.3 s to 0.312 s. The T_e perturbation due to the TM also had an increasing oscillation period (Fig. 3 (*e*)). After 0.312 s, f_{TM} decreased to around 30 Hz, estimated by the evolution of $\varphi^{n=1}$ (Fig. 3 (*d*)) which varied by 220^o between 0.312 s and 0.333 s. $b_r^{n=1}$ (Fig. 3 (*d*)) also grew fast. Due to this slowly rotating TM, the T_e signals (Fig. 3 (*e*)) were also modulated at around 30 Hz. They measured the O-point of the TM at 0.312 s when the radial T_e profile was flattened near the RS, and the X-point at 0.321 s when the radial T_e gradient was large. These observations indicate that the TM was locked towards the wall/error field from 0.312 s. Hereafter, the TM with f_{TM} < 0.1 kHz is referred to as a quasi-static TM (QSM).

The evolution of the magnetic perturbation at f_{RRMP} (referred to as “plasma response” in this paper) can be clearly observed since 0.3 s from the power spectrum of Mirnov signal shown in Fig. 3 (*c*). It is noted that the vacuum magnetic field measured by Mirnov probe directly from the RRMP coils is more than one order smaller than the magnetic perturbations due to plasma response to RRMP. The amplitude of the plasma response changed significantly during the QSM phase and the response, measured by $\delta b_\theta(f_{RRMP})$, even disappeared dramatically at around 0.312 s and around 0.326 s (Fig. 3 (*b*) and (*c*)). This is related to the QSM phase and will be described in detail in Fig. 5. As shown in Fig. 3 (*d*), the T_e perturbations, measured at f_{RRMP}, also show the dependence of the plasma response on the QSM phase. At R_{ECE} = 91.1 cm (radially inside the RS), the T_e perturbation at f_{RRMP} was quite small at the O-point (0.312 s) and X-point (0.321 s) of the QSM, while it had a maximum between

O- and X- points. An expanded view of the gray dashed rectangle marked in Fig. 3 (*e*) is shown in Fig. 4(*a*) for the 4 T_e signals measuring near the magnetic island. The phases of the T_e perturbations at 6 kHz are opposite between channels measured inside and outside the radial location of 2/1 RS (e.g. R_{ECE} = 89.3 cm versus 84.5 cm), as marked by the gray vertical-dashed lines at around 0.326s in Fig. 4(*a*). At t_1 (or t_2), the T_e measured at 87.6 cm (or 84.5 cm) decreased (or increased) to the same value as that measured at 86 cm. This indicates that the ECE signals began to measure inside the separatrix of the island since t_1 at 87.6 cm and since t_2 at 84.5 cm. Simultaneously, the T_e perturbations at 6 kHz disappeared.

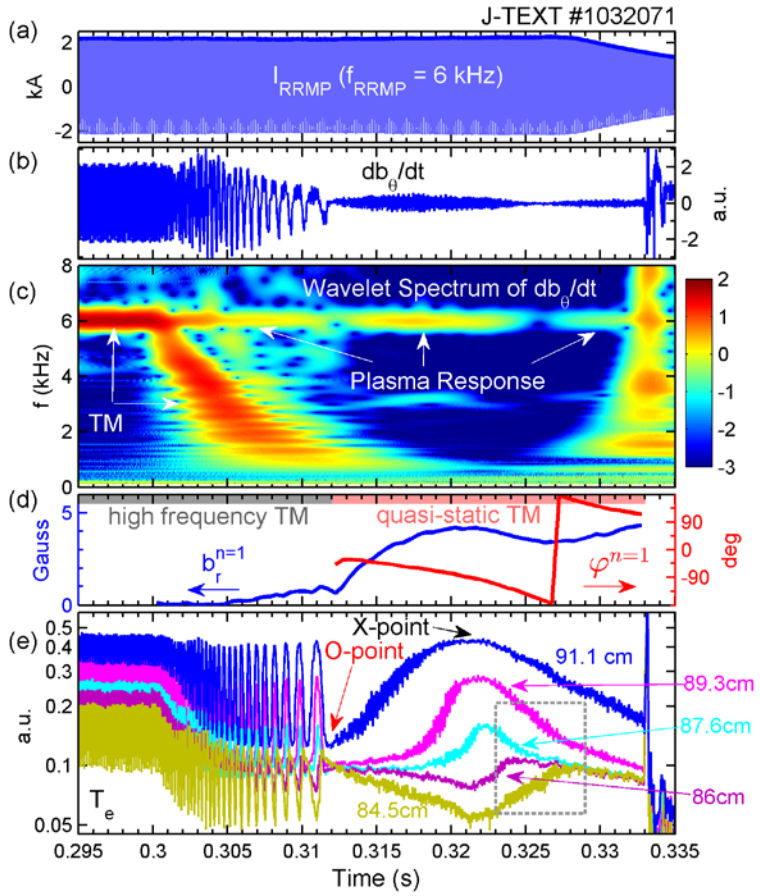

Fig. 3 The plasma response to a RMP rotating at 6 kHz with a quasi-static TM in J-TEXT discharge #1032071. From top to bottom, (*a*) The RRMP coil current, (*b*) the Mirnov coil signal measured at $\theta = 0^o$, (*c*) the wavelet power spectrum of Mirnov signal, (*d*) the amplitude (blue, left vertical axis) and phase (red, right vertical axis) of the $n = 1$ radial field measured by the LMDs, (*e*) T_e measured at various radial locations around 2/1 RS.

Also shown in Fig. 4(*a*) is T_e^{ave}, the averaged T_e calculated for a set of time windows with the duration of $2/f_{RRMP} \approx 0.33$ ms. The measured T_e consists of 3 components, i.e. the equilibrium component with $m/n = 0/0$, $T_e^{0/0}$, the 2/1 component varied at ~30 Hz due to the 2/1 TM, $T_e^{2/1}$, and the high frequency component due to the plasma response, $\delta T_e(f_{RRMP})$. For this current case with a QSM, the time resolution of T_e^{ave}, 0.33 ms, is high enough to describe $T_e^{2/1}$, hence $T_e^{ave} = T_e^{0/0} + T_e^{2/1}$. The evolution of T_e^{ave} versus time and radial location is shown in Fig. 4(*b*) by the contour lines. The full contour lines with the values of 0.09 and 0.11 indicate the magnetic island region. The O-/X-points are marked in Fig. 4(*b*). $\delta T_e(f_{RRMP})$, calculated every 0.33 ms, is also shown in Fig. 4(*b*) by the

scatter plots. The color represents the ratio between δT_e and $<\delta T_e>$, the mean of T_e during the whole QSM stage, and the gray indicates a very small (<2%) plasma response. It is clearly shown that the T_e perturbations due to plasma response are approximately zero (gray solid circles) inside the magnetic island or outside the magnetic island at $\theta = \theta_O$ or θ_X in discharge #1032071, where θ_O and θ_X are the poloidal positions of the O- and X- points respectively.

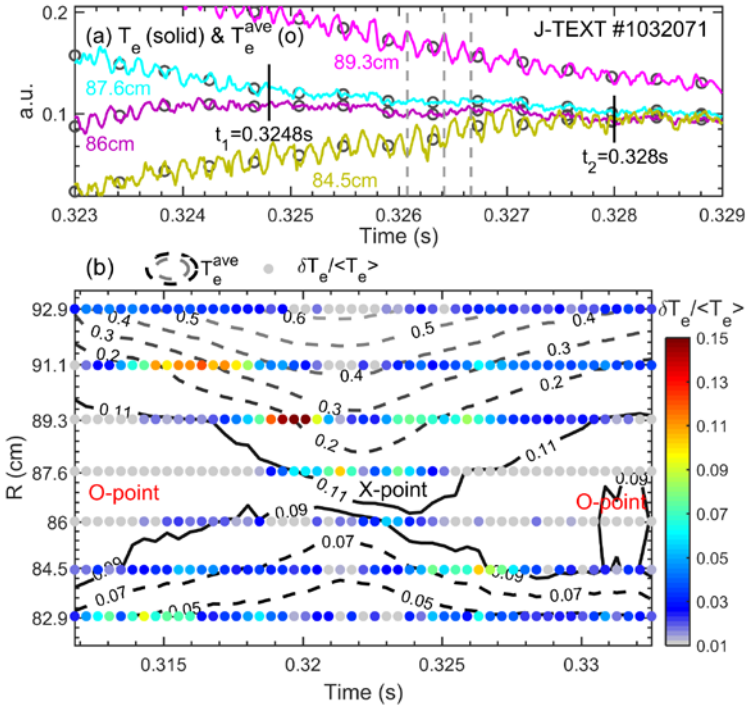

Fig. 4 The plasma response to RRMP measured from electron temperature during the QSM phase in discharge #1032071. (*a*) The evolution of T_e measured at 4 radial locations corresponding to the gray dashed rectangle marked in Fig. 3 (*e*). The averaged T_e during every two periods of the RRMP, T_e^{ave}, are also shown by the gray circles. (*b*) The dependence of plasma response, $\delta T_e(f_{RRMP})/<T_e>$, and T_e^{ave} on the time and radial locations are shown by the scatter plot and contour lines respectively. $<T_e>$ is the mean of T_e from 0.312 s to 0.332 s at each radial location.

Fig. 5 displays the time evolution of the magnetic perturbation due to plasma response during the QSM phase. Each blue curve represents the magnetic perturbation, δb_θ, measured at f_{RRMP} by one Mirnov probe and is centered at its poloidal location. The poloidal positions of the QSM O-points at φ_{Mir} are $\theta_O = (\xi_O^{2/1} - n\varphi_{Mir} + k\pi)/m = (\varphi^{n=1} + 90^o - \varphi_{Mir} + k\pi)/2$ with k = 0, 2, while the poloidal positions of the X-points, θ_X, equal to $\theta_O - \pi/m$. The time evolution of θ_O and θ_X are shown by the red and black lines respectively in Fig. 5(*a*). As seen from Fig. 5(*a*), there are always 4 poloidal locations where the magnetic perturbations were almost zero, hereafter these locations are referred to as θ_{min}. θ_{min} decreased in a similar manner as θ_O and θ_X, which reflect the rotation of the QSM. Especially, θ_{min} is approximately equal to θ_O or θ_X. The three expanded views (Fig. 5(*b*), (c) and (*d*)) show more clearly that the magnetic perturbations at f_{RRMP} measured around the O-/X- points of the QSM were quite small.

The magnetic perturbations, measured at $\theta \neq \theta_O$ and θ_X, are much larger. And their phases at various poloidal locations are exactly the opposite (the same) for channels in the different sides (the same side) of the O-/X- points. For example, the δb_θ signals measured at $\theta \in [\theta_{X1}, \theta_{O1}]$ have the same

oscillation phase in Fig. 5(d), while they have the opposite phase with those δb_θ signals measured at $\theta \in [\theta_{O1}, \theta_{X2}]$. These features were also observed from the toroidal Mirnov array with two minima observed toroidally, hence the poloidal/toroidal mode numbers of the plasma response are m/n = 2/1.

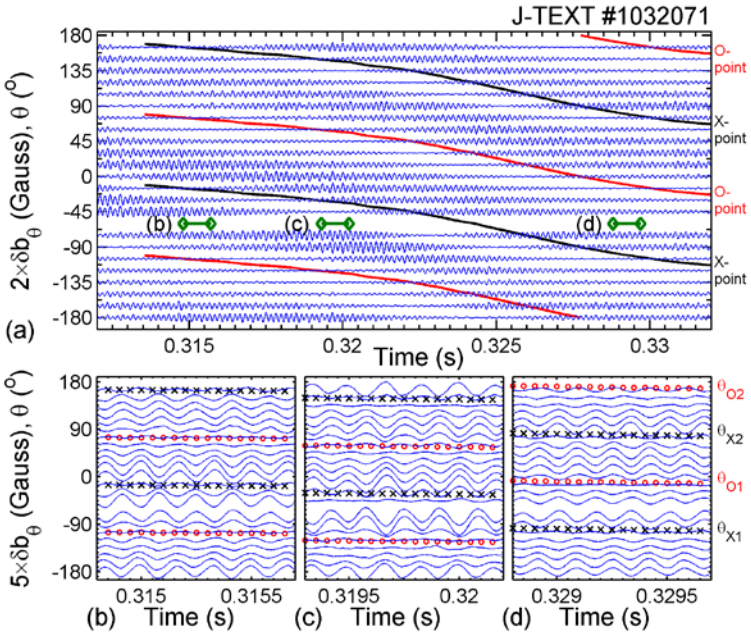

Fig. 5 The time evolution of magnetic perturbations measured at f_{RRMP} = 6 kHz, with each signal centered at its poloidal position. (*a*) overview of the response, (*b*) to (*d*) expanded views of (*a*) for those durations marked by the dark green lines at θ = - 60° in (*a*). The poloidal locations of the QSM O-/X-points at φ_{Mir}, calculated from $\varphi^{n=1}$ (Fig. 3 (*d*)), are marked by the red and black lines in (*a*) and by red circles and black crosses in (*b*) to (*d*).

The above features of magnetic perturbations could be roughly described by the formula $\delta b_\theta(\theta, t) = 2A sin(m\theta - m\theta_O)cos(2\pi f_{RRMP}t)$, which is usually used to describe a standing wave. Hence these features are referred to as "*standing wave like*" features in this paper, and the locations with minimal magnetic perturbations are referred to as "*nodes*". It is noted that the *standing wave* and *nodes* are defined in the TM rest frame, since θ_O varies together with the rotation of TMs.

This kind of *standing wave like* plasma response, which strongly related to the structure of magnetic island, has not been reported previously. It is important to understand the mechanism behind it. This could not be due to the rotating TM induced by RRMP at $q \neq 2$, since T_e perturbations are measured at around the separatrix of 2/1 TM and magnetic perturbations are measured with m/n = 2/1. The formation of an additional island due to RRMP at the 2/1 RS, as observed in TEXTOR [34], might be an explanation. However, the formation of a secondary island needs a very large island size, and it will be shown in the next sub-section that the plasma response described in this paper does not need a very large island. In Section 4 and 5, it is shown that the RRMP can drive the phase oscillation of the TM by applying a periodical electromagnetic torque and that the phase oscillation of the TM can induce the plasma response described above. To compare with the modelling results, the dependences of plasma response on plasma and RRMP parameters are investigated quantitatively in Section 3.3.

3.3. Dependences of the plasma response to RRMP on the locked mode phase and the RRMP amplitude

A set of dedicated experiments has been carried out to investigate the plasma response to RRMP quantitatively, as listed in Table 1. The effect of the locked mode phase on the plasma response is compared between case 1 and case 2. The phases of LMs, $\varphi^{n=1}$, were maintained at two different values in case 1 and 2 by applying SRMP fields at two different phases, $\delta_{SRMP}^{2/1}$. The plasma response to RRMP without large tearing mode was investigated in case 3, which has been briefly described in Section 3.1 and will be compared to case 1 and 2 in the next section. The RRMP was applied with f_{RRMP} = 4 kHz. In each case, the dependence of plasma response on the RRMP amplitude was carried out by scanning I_{RRMP} from 0 to 5 kA.

Table 1. Table of dedicated cases for investigating the plasma response to RRMP with a locked mode and without tearing mode.

Case	f_{RRMP} (kHz)	Static RMP		Locked mode phase ($\varphi^{n=1}$)	Discharges
		$\delta_{SRMP}^{2/1}$	I_{SRMP} (kA)		
1	4	290^o	1.2	$25^o \pm 5^o$	1032000+ {183, 187, **192**, 193, 194, 200}
2	4	110^o	3.0	$145^o \pm 5^o$	1032000+ {492, 493, **502**, 503}
3	4	w/o	w/o	w/o TM	1032000+ {161, 163, 165, 166, **189**}

Fig. 6 displays a direct comparison of two typical discharges from case 1 (#1032192, blue solid lines) and case 2 (# 1032502, red dashes lines). The SRMP coils were fed with DC current to generate a 2/1 SRMP field (Fig. 6(*a*)). With the ramp-up of the SRMP field, the rotating TM was locked to a fixed position. Once the TM was locked, the SRMP field was reduced to a lower value which was sufficient to maintain the locking of TM but wasn't sufficient to cause disruption. The phases of 2/1 SRMP, $\delta_{SRMP}^{2/1}$, were set to be 290^o (#1032192, case 1) and 110^o (#1032502, case 2) respectively, so that the LMs were maintained at different toroidal positions (Fig. 6(*c*)). Due to the intrinsic 2/1 error field (EF) at a phase of $\delta_{EF}^{2/1} \sim 317^o$ [49], higher SRMP currents were needed for case 2 to lock and maintain the 2/1 locked mode compared to case 1. As a result, the locked modes were obtained at the amplitudes $b_r^{n=1} \approx$ 2.6 - 3 Gauss and $b_r^{n=1} \approx$ 3 - 3.5 Gauss and the phases $\varphi^{n=1} \approx 25^o \pm 5^o$ and $\varphi^{n=1} \approx 145^o \pm 5^o$ for case 1 and case 2, respectively.

The RRMP fields were applied by feeding the RRMP coils with 4 kHz AC currents (envelopes shown in Fig. 6(*a*)), after the phases and the amplitudes of locked modes reached their stationary values. As soon as the RRMP field was applied, the plasma response at f_{RRMP} can be observed from the power spectrum of Mirnov signals (Fig. 6(*e*) and (*f*)). The effect of the LM phase on plasma

response already appeared as the b_θ response of #1032502 was significantly smaller than that of #1032192. Besides, after the application of the RRMP, the phase of $b_r^{n=1}$ (Fig. 6(*c*)) decreased slightly towards the initial TM rotation direction, i.e. $\varphi^{n=1} \approx 5^o$ and $\varphi^{n=1} \approx 140^o$ in #1032192 and #1032502 respectively. Then the position of the 2/1 LM in #1032502 is shifted by $\Delta\theta_{LM} = +67.5^o$ poloidally with respect to that of #1032192.

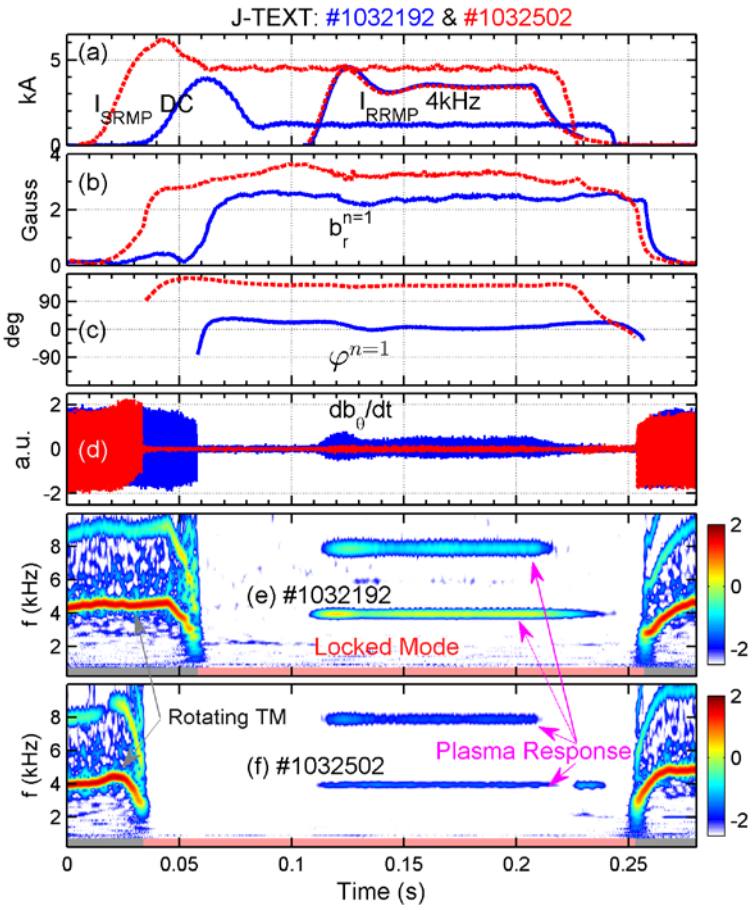

Fig. 6 Comparison of the plasma response to RRMP for two discharges with different locked mode positions. From top to bottom, (*a*) the SRMP coil currents and the envelope of RRMP coil currents, (*b*) the amplitude and (*c*) the phase of the $n = 1$ radial field measured by the LMDs, (*d*) Mirnov signals, db_θ/dt, measured at $\theta = 0^o$ and (*e*), (*f*) the wavelet power spectrum of db_θ/dt for #1032192 (case 1, blue solid lines) and #1032502 (case 2, red dashes lines).

Fig. 7 shows the poloidal distributions of the magnetic perturbations due to plasma responses for #1032192 and #1032502. The amplitudes of the magnetic perturbations are shown at f_{RRMP} [$\delta b_\theta(f_{RRMP})$, Fig. 7 (*a*)] and $2f_{RRMP}$ [$\delta b_\theta(2f_{RRMP})$ normalized to $\delta b_\theta(f_{RRMP})$ in Fig. 7 (*c*) and $\delta b_\theta(2f_{RRMP})$ in Fig. 7 (*d*)], which are calculated as described in the end of Section 2. The phases of the plasma response at 4 kHz with respect to the phase of the AC current in one of the RRMP coil, $\Delta\phi(f_{RRMP}) = \phi_{b\theta}(f_{RRMP}) - \delta_4$, are shown in Fig. 7 (*b*). Four clear peaks of $\delta b_\theta(f_{RRMP})$ can be observed with each peak covering ~ 90^o poloidally from Fig. 7 (*a*). The corresponding $\Delta\phi(f_{RRMP})$ kept the same for each peak and showed 180^o phase reversal between adjacent peaks.

Shifting the *nodes* of the magnetic perturbations in #1032192 by $+67.5^o$ poloidally, it will match the location of the *nodes* in #1032502. Hence the relationship that the *nodes* of the response located

near the O-/X- points of the TM is verified again. Yet the phase difference [$\Delta\phi(f_{RRMP})$, Fig. 7 (*b*)] can't match between these two discharges after the shifting of #1032192. This mismatch will be discussed in section 6, and it will show that it doesn't have to be conflicting to the conclusion that the *standing wave like* structure have clear relationship to the structure of locked mode.

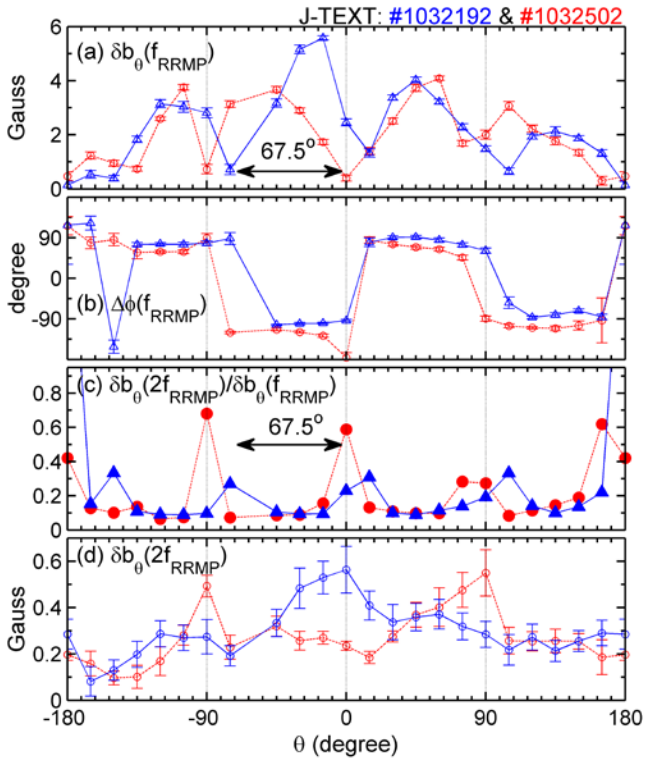

Fig. 7 The poloidal distribution of magnetic perturbations due to plasma response measured by the poloidal Mirnov array during the flattop of the 4 kHz RRMP in #1032192 (blue solid lines) and #1032502 (red dashes lines). (*a*) The amplitudes, $\delta b_\theta(f_{RRMP})$, and (*b*) the phases, $\Delta\phi(f_{RRMP})$, at f_{RRMP} = 4 kHz, (*c*) the ratio between $\delta b_\theta(2f_{RRMP})$, the amplitudes at $2f_{RRMP}$, and $\delta b_\theta(f_{RRMP})$, (*d*) $\delta b_\theta(2f_{RRMP})$. An average during the flattop of the RRMP was taken. The phases of the magnetic perturbations were measured with respect to the phase of the AC current in one of the RRMP coil, i.e. δ_4 as shown in Fig. 1.

Fig. 7(*c*) shows that there are peaks of $\delta b_\theta(2f_{RRMP})/\delta b_\theta(f_{RRMP})$ near each node where $\delta b_\theta(f_{RRMP})$ is minimal, e.g. at θ = -90° in #1032502. It is noted that these peaks appeared not only due to $\delta b_\theta(f_{RRMP})$ approaching to zero but also because $\delta b_\theta(2f_{RRMP})$ being very large at these locations, as shown in Fig. 7(*d*). Fig. 8 displays the time evolution of δb_θ, obtained by integrating db_θ/dt numerically and applying a high pass filter with the cut-off frequency of 1 kHz, for discharge #1032502. It is found that the phases of the magnetic perturbations at 4 kHz are opposite between δb_θ measured at θ = -75° and -105°, e.g. at t = 0.12344 s. δb_θ measured at θ = -90° showed a clear component at $2f_{RRMP}$ with two features: (i) all its peaks were corresponding to the peaks or the dips of δb_θ at θ = -75° and -105°, and (ii) all its dips were located somewhere in between. This feature, that $\delta b_\theta(2f_{RRMP})$ appeared with a strong amplitude at where $\delta b_\theta(f_{RRMP})$ is minimal and $\Delta\phi(f_{RRMP})$ reversed, is different from the standing wave and is an important feature of the forced phase oscillation of the TM due to the RRMP. We will explain this in Section 4 and 5.

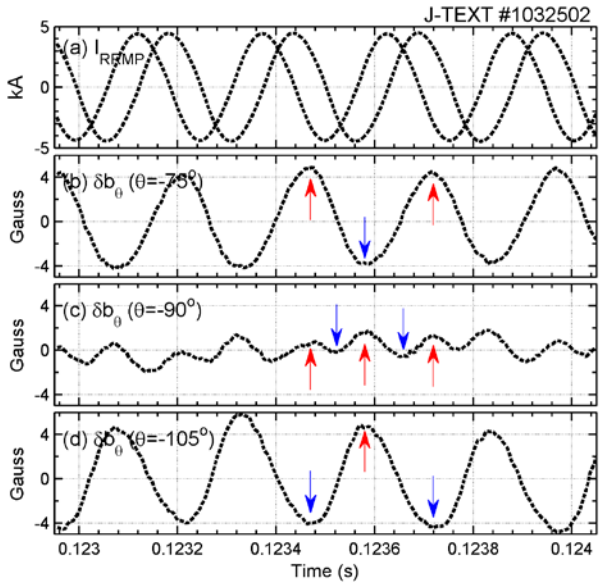

Fig. 8 The time evolution of (*a*) I_{RRMP} and (*b*) to (*d*) the high frequency component of the perturbed b_θ, δb_θ, measured by the poloidal Mirnov array at θ = -75°, -90° and -105° in discharge #1032502. The peaks and dips of δb_θ are marked by red and blue arrows respectively.

Fig. 9 displays the dependence of the plasma response amplitude on the RRMP amplitude, which is obtained by scanning I_{RRMP} in the 3 cases shown in Table 1. The amplitudes of plasma responses were measured by the maximum of $\delta b_\theta(f_{RRMP})$ among the poloidal channels, max[$\delta b_\theta(f_{RRMP})$] shown in Fig. 9(*a*), and $\delta T_e(f_{RRMP})$ shown in Fig. 9(*b*), respectively. It is found that the amplitude of magnetic perturbation increased linearly with I_{RRMP} and the response in case 1 was larger than that of case 2.

Fig. 9(*b*) shows the electron temperature perturbation, $\delta T_e(f_{RRMP})$, measured by ECE signals at ξ_{ECE} = 90°. According to Table 1, the distances between the ECE measured location and the O-points of the locked modes were $\xi_{ECE} - \xi_O^{2/1} = \xi_{ECE} - (\varphi^{n=1}+90^o) = -\varphi^{n=1} \approx -25^o \pm 5^o$ for case 1 and $-145^o \pm 5^o$ for case 2, respectively. This indicates that the ECE measured the plasma response near the O-point and the X-point of the locked mode in case 1 and case 2. This is confirmed by the measured radial profile of T_e^{ave} which was flattened for more than 3 channels near 88 cm (the location of the 2/1 RS at HFS) in #1032192 and was less flattened in #1032502. In case 2, $\delta T_e(f_{RRMP})$ increased linearly with I_{RRMP} at R = 91 cm (Fig. 9(*b*)) and R = 89.2 cm (not shown here), which were both outside the separatrix of the LM at $\xi_{ECE} - \xi_X^{2/1} \approx 35^o \pm 5^o$. In case 1, $\delta T_e(f_{RRMP})$ measured at R = 91 cm, which was outside the separatrix of the LM at $\xi_{ECE} - \xi_O^{2/1} \approx -25^o \pm 5^o$, showed a similar dependence as $\delta T_e(f_{RRMP})$ at R = 91 cm of case 2. In case 1, $\delta T_e(f_{RRMP})$ measured inside the separatrix of the LM, i.e. at R = 89.2 cm, were quite small, although they also increased with I_{RRMP} at a very small rate. Since $|\xi_{ECE} - \xi_X^{2/1}|$ and $|\xi_{ECE} - \xi_O^{2/1}|$ were around 25°~35° in case 1 and 2, the T_e perturbations due to the plasma responses were large outside (respectively were almost zero inside) the separatrix of the island. This is consistent with the results described in Fig. 4.

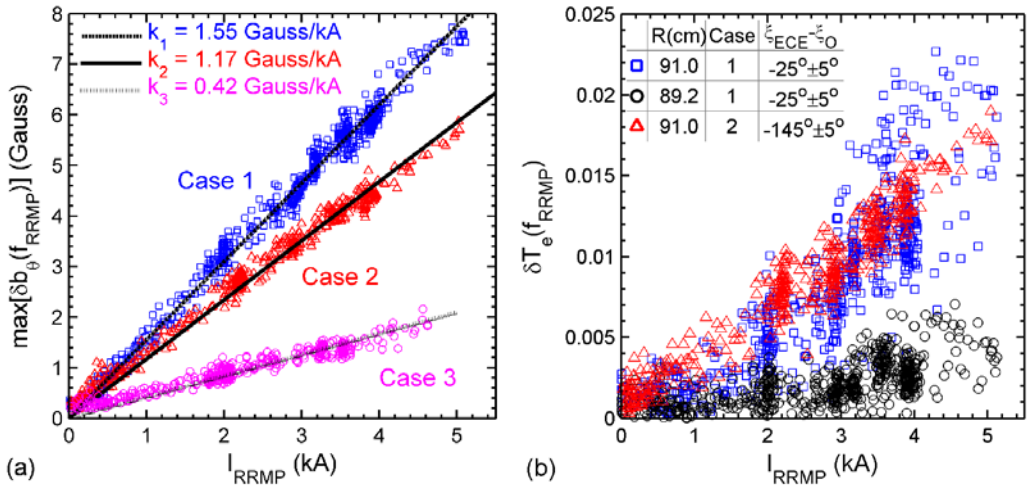

Fig. 9 The dependence of the plasma response amplitude on the RRMP amplitude (represented by the RRMP current). (*a*) The amplitude of magnetic perturbation is represented by the maximum of $\delta b_\theta(f_{RRMP})$ among the poloidal channels, max[$\delta b_\theta(f_{RRMP})$], for case 1, 2 and 3. k_i (i = 1, 2 and 3) is the mean of max[$\delta b_\theta(f_{RRMP})$]/$I_{RRMP}$. (*b*) T_e perturbation, $\delta T_e(f_{RRMP})$, is shown for the ECE channels measured at R = 91.0 cm and 89.2 cm in case 1 and R = 91.0 cm in case 2.

3.4. Comparison and brief summary of the measured plasma response to RRMP with locked mode and without tearing mode

It is important to find as many evidences as possible that can explain the *standing wave like* feature of the plasma response to RRMP with a QSM/LM. These features are different from those of the screening effects. But there should be screening effect at the 2/1 RS which also contributed to part of the plasma response in case 1 and 2, because the slip frequency f_s = -4 kHz due to the presence of the locked 2/1 mode (f_{MHD} = 0).

To estimate the amplitude of the screening effect in case 1 and 2, a set of *tearing-stable* discharges (case 3 in Table 1) was carried out with similar $|f_s|$ and resistivity at the 2/1 RS as those of case 1 and 2. In case 3, f_s was around 4 kHz at the 2/1 RS, by applying RRMP with f_{RRMP} = 4 kHz to discharges with 2/1 SMOs at $f_{MHD} \approx 8$ kHz. The resistivity at the 2/1 RS were also similar from case 1 to 3, by keeping the constant I_p, B_t, and the similar electron density and T_e. As a result, the degrees of the screening could vary slightly between the cases with LM and the cases without TM, but their amplitudes should be comparable. Fig. 9 (*a*) shows that the amplitude of plasma response in case 3 increased linearly with RRMP, but with much smaller amplitude compared to that of case 1 and 2. As discussed in Section 3.1, the dominate plasma response in case 3 was from the 3/1 RS, while the screening effect from the 2/1 RS only contributed a small component. Hence, the screening effect from the 2/1 RS only contributed to a very small proportion of the measured plasma response in the

cases with a QSM/LM.

As mentioned previously, it will show by a phenomenological model in section 4 and by numerical modeling in section 5 that the phase oscillation of LMs due to RRMP could induce the observed *standing wave like* plasma response. For the convenience of the comparison, we briefly summarize the features of the plasma response to RRMP for cases without TM and with LMs as follows.

The plasma response in a *tearing-stable* plasma showed a feature of travelling wave. Its dominant poloidal mode number *m* equaled 3, indicating that it originated mainly from 3/1 RS.

After applying the RRMP field to the plasmas with a QSM/LM, the plasma responses to RRMP were measured with the following features:

(1) The magnetic perturbations had a *standing wave like* structure in the TM rest frame, including:
   a) Four and two *nodes* of the response can be observed poloidally and toroidally, respectively. They were located around the O-/X- points of the 2/1 TM. The magnetic perturbation measured near the *node* had a large $\delta b_\theta(2f_{\mathrm{RRMP}})$ component, while the $\delta b_\theta(f_{\mathrm{RRMP}})$ component was almost zero.
   b) The magnetic perturbation measured at two channels between two adjacent *nodes* were in phase, but their phases were reversed between two channels on different side of a *node*.

(2) The T_e perturbation were zero or minimal inside the locked island or outside the magnetic island but at the same poloidal positions as the O-/X- points. The phases of the T_e perturbation are opposite between channels inside and outside the 2/1 RS.

(3) Both the T_e and b_θ perturbations increased linearly with the RRMP field.

4. Phenomenological model

The standing wave like feature of the plasma response with a locked TM is not due to the screening effect at the RS, as discussed in section 3.4. In the presence of a locked TM, the effect of the RRMP on the TM should be considered as well.

The applied 2/1 RMP has two effects [5, 6] on the 2/1 TM: (a) it modifies the stability of the TM by adding an additional tearing stability index

$$\Delta'_{RMP} = \frac{2m}{r_s}\left(\frac{W_{vac}}{W}\right)^2 \cos(\Delta\xi), \qquad (1)$$

and (b) it applies an electromagnetic $\boldsymbol{J}\times\boldsymbol{B}$ torque on the mode, with the toroidal component in the form of

$$T_{RMP,\Phi} = -\frac{4mn\pi^2 R_0}{\mu_0}|\Psi_{vac}\|\Psi|\sin(\Delta\xi), \quad (2)$$

where r_s is the radial coordinate of the RS and R_0 the major radius. In equation (1) W is the full island width and W_{vac} is the vacuum island width. They are proportional to the square root of the reconnected flux $|\Psi|$ and of $|\Psi_{vac}|$, respectively. $|\Psi_{vac}|$ is the helical flux induced by RMP at $q = m/n$ surface in the absence of a plasma, i.e. vacuum, hence it is proportional to the RMP amplitude. $\Delta\xi$ is the phase difference between the phase of TM, ξ_O or ξ_{TM}, and the phase of RMP, $\xi_{O,\,vac}$.

When the TM is locked to the wall, the EF or the externally applied SRMP, the phase difference between the RRMP and the locked mode will be $\Delta\xi = \xi_{TM} - \xi_{RRMP} \approx \xi_0 - 2\pi f_{RRMP}t$. As a result, the RRMP will apply a periodic torque on the LM at the frequency of f_{RRMP}. This oscillating torque will drive the phase of the LM to oscillate at f_{RRMP} around its initial locking location. A simplified phenomenological model is used to describe the forced phase oscillation of the LM and to investigate the features of the corresponding plasma response.

In a cylinder coordinate, the perturbed non-axisymmetric poloidal magnetic field generated by the LM can be described by

$$b_\theta^{2/1} = b_{O-point} \times \cos(\xi - \xi_{O-point}). \quad (3)$$

When the RRMP is applied and leads to the forced phase oscillation of the LM around its original locked position, the rotation velocity of the TM could be described by

$$\omega(t) = \omega_0 + \omega_1 \cos(2\pi f_{RRMP}t + \phi_{\omega 1}) + \omega_2 \cos(2\pi \times 2f_{RRMP}t + \phi_{\omega 2}) + \ldots, \quad (4)$$

where ω_0 is 0 for a locked mode. Then the phase evolution of the locked mode could be obtained by

$$\xi_{O-point}(t) = \xi_0 + \int_0^t \omega(t)\,dt, \quad (5)$$

where ξ_0 is the location of O-point at $t = 0$. Considering that the island width could also be modified by the applied RRMP, we describe the island width as

$$W(t) = W_0 + W_1 \cos(2\pi f_{RRMP}t + \varphi_{W1}) + \ldots, \quad (6)$$

With all these assumptions, the non-axisymmetric magnetic field generated by the island can be described by

$$b_\theta(\xi, t) = k \times W(t)^2 \times \cos(\xi - \xi_{O-point}(t)), \quad (7)$$

where k is the ratio of magnetic field generated by unit island width.

To further simplify the model, the variation of the island width is neglected, and all the harmonics

of ξ_{TM} which are higher than f_{RRMP} are omitted. Hence only the effect of the forced phase oscillation is considered and the corresponding plasma response is shown in the schematic diagram in Fig. 10. The helical coordinate ξ and ξ' are defined in the laboratory frame and in the island rest frame respectively in Fig. 10. The coordinate transformation is given by $\xi' = \xi - \xi_{TM}$, so that the island phase, $\xi'_{TM}(t)$, is 0 in the island rest frame. Fig. 10(*a*) shows the perturbed flux surfaces illustrating the island structure in the ξ'-*r* panel, while the corresponding perturbed poloidal magnetic field, $b_\theta^{2/1}(\xi')$, is shown in Fig. 10(*b*). Fig. 10(*c*) shows the time evolution of the location of island O-point in the laboratory frame, ξ_{TM}. ξ_{TM} is set to be 0 in the beginning, and then forced to oscillate at f_{RRMP} from t = 0.5, i.e. $\xi_{TM}(t>0.5) = \delta\xi_{TM}\times\sin[2\pi(t - 0.5)]$, where $\delta\xi_{TM}$ is the oscillation amplitude of ξ_{TM} with a value of 0.1. Three test probes are placed at ξ_{Probe} = -0.3, 0 and 0.15 to illustrate the measured magnetic fields, b_θ^{Probe}, due to the oscillation of ξ_{TM}. b_θ^{Probe} measured in the laboratory frame is the same as that measured in the TM rest frame, where $\xi'_{TM}(t) = 0$ and the probe locations $\xi'_{Probe}(t) = \xi_{Probe} - \xi_{TM}$. So the probe locations ξ'_{Probe} oscillate from 0.5 as shown in Fig. 10(*d*). As a result, b_θ^{Probe} also change as shown in Fig. 10(*f*).

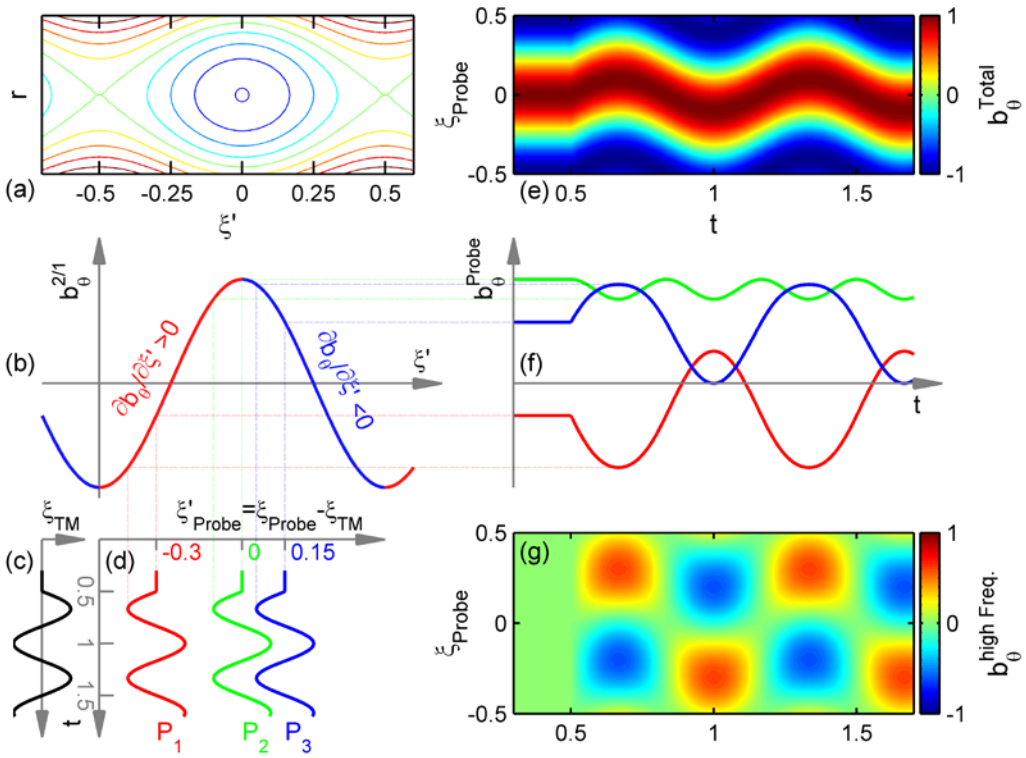

Fig. 10 Schematic diagram of the plasma response to the phase oscillation of locked tearing mode. (*a*) the perturbed flux surfaces of locked TM in ξ'-*r* panel, where ξ' is the helical coordinate in the TM rest frame; (*b*) the distribution of the perturbed poloidal field by TM, $b_\theta^{2/1}(\xi')$; (*c*) the evolution of TM phase, ξ_{TM}, in the laboratory frame; (*d*) the locations of test probes in the TM rest frame, ξ'_{Probe}; (*f*) the measured poloidal field by the test probes shown in (*d*); (*e*) the total and (*g*) the high frequency component of the measured b_θ^{Probe}

versus time and ξ_{Probe}.

When ξ_{TM} begins to increase at t = 0.5, ξ'_{Probe} decrease for all the probes (Fig. 10(*d*)). And b_θ^{Probe} decreases at P_1 and increases at P_3 (Fig. 10(*f*)), since the perpendicular gradient of b_θ ($\partial b_\theta/\partial\xi'$) is positive ($P_1$) and negative ($P_3$) respectively. $b_\theta^{2/1}$ is monotonous in the region where P_1 or P_3 measures, hence b_θ^{Probe} has a dominant frequency at f_{RRMP}. The phases of the measured b_θ perturbations are opposite if they are measured in different sides of the O- or X- points. When $\delta\xi_{\text{TM}}$ is larger than the distance between the probe and the O- or the X- point of TM at t =0, i.e. $\delta\xi_{\text{TM}} > |\xi'_{\text{probe}} - \xi'_{\text{o-point}}(0)|$ or $\delta\xi_{\text{TM}} > |\xi'_{\text{probe}} - \xi'_{\text{x-point}}(0)|$, the probe measures both sides of the O-point or X-point of the TM within one oscillation cycle. The change of the sign of $\partial b_\theta/\partial\xi'$ will then contribute to additional changes of b_θ^{Probe}, and hence produces a large component of b_θ at $2f_{\text{RRMP}}$, as illustrated by P_2 (green lines) in Fig. 10(*d*) and Fig. 10(*f*). The total and the high frequency part of b_θ^{Probe} are shown in Fig. 10(*e*) and Fig. 10(*g*). These features of b_θ^{Probe} are in good agreement with those listed in section 3.4 for the b_θ perturbation due to plasma response in the experiments.

According to the above analysis, the high frequency plasma response due to the forced phase oscillation of the TM originates mainly from the poloidal gradient of the perturbed non-axisymmetric parameters by the TM.

This is also appropriate for the T_e perturbation. The poloidal gradient of T_e, $\partial T_e/\partial\xi$, is opposite in both sides of the O- / X- point and has maxima (minima) in between (at) O- / X- points. Hence, the response is maximal (minimal) in between (at) O- / X- point. Since the temperature within the separatrix of island is rather flat in an Ohmic plasma which has no additional heat source inside the island [50], the T_e perturbations due to forced phase oscillation will disappear inside the separatrix of the TM. The T_e gradients, $\partial T_e/\partial\xi$, have different signs inside and outside of the RS, hence the phases of the T_e perturbations reverse correspondingly.

The poloidal maximum of $\delta b_\theta(f_{\text{RRMP}})$ locates at the maximum of $\partial b_\theta/\partial\xi'$, such as ξ' = -0.25 and 0.25 in Fig. 10(*b*), and its amplitude is

$$\delta b_\theta^{\max} = b_{O-point} \times \sin(\delta\xi_{TM}). \tag{8}$$

When the applied RRMP field is very small, $\delta\xi_{\text{TM}}$ should also be very small, and hence $\delta b_\theta^{\max} \approx b_{\text{O-point}} \times \delta\xi_{\text{TM}}$. If

$$\delta\xi_{\text{TM}} \propto I_{RRMP}, \tag{9}$$

then

$$\delta b_{\theta}^{max} \propto I_{RRMP}, \quad (10)$$

as shown experimentally in Fig. 9(*a*). To prove whether Eq. (9) is true or not, the equation of the torque balance of the island has to be solved numerically. This won't be conducted in this paper; instead, Eq. (9) will be tested in Fig. 13 of section 5 by solving the reduced MHD equations using the non-linear code TM1. Note that for a small $\delta\xi_{TM}$, the amplitude of plasma response is

$$\delta A = -\partial A / \partial \xi \times \delta\xi_{TM}, \quad (11)$$

where A represents $b_{\theta}^{m/n}$ or $T_e^{m/n}$. The minus indicates that the plasma response is out of phase with the TM phase oscillation if $\partial A/\partial\xi > 0$.

As described above, the forced phase oscillation of locked mode by RRMP can produce the plasma response with all the experimentally observed features as summarized in section 3.4, qualitatively. A further investigation of this effect will be carried out quantitatively by using a nonlinear numerical code, as shown in section 5.

5. Numerical results

To understand the plasma response to RRMP with a locked TM as described experimentally in section 3 and discussed phenomenologically in section 4, a nonlinear numerical modeling based on reduced MHD equations has been carried out using the low-β and large aspect-ratio approximation. The Ohm's law and the equation of motion are the basic equations in the modeling. The effect of a single helicity RMP with m/n = 2/1 is taken into account by the boundary condition $\psi_{2/1}(r = a) = \psi_a a B_t \cos(m\theta+n\varphi)$, where ψ_a describes the normalized m/n = 2/1 helical magnetic flux amplitude at $r = a$. The radial magnetic field perturbation at $r = a$ is given by $b_{ra} = m\psi_a B_t$. The single-fluid equations are solved simultaneously using the initial value code TM1, which has been used for modeling the nonlinear growth and saturation of neoclassical TMs [51], their stabilization by radio frequency (RF) current [29], and the effect of RMP on resistive TM [6, 52]. The parameters are calculated at $\varphi = 0$ in the modeling, hence the coordinate $\xi = m\theta$. The phase of the TM is defined by its phase at the O-point, i.e. $\xi_{TM} = \xi_{O\text{-point}}$. The phase of the RMP field, ξ_{RMP}, is defined by the phase of the maximal $\psi_{2/1}$, which also corresponds to the O-point phase of the vacuum island.

It should be mentioned that the diamagnetic drift has not been included in the modeling results shown in this paper. For the low-β J-TEXT plasma with a large island, the effect of the diamagnetic drifts is weak due to the pressure flattening across the island [53]. In addition, the interaction between RMP and 2/1 TM modeled previously by using two fluid equations showed similar results to

that obtained by single fluid equations [54]. So it is approximate to interpret the plasma response to RRMP with the presence of a large TM by using the single fluid model.

The input parameters for the numerical modeling are based on the J-TEXT experimental parameters as presented in section 3. A monotonic profile for safety factor q is taken with the q = 2 surface located at 0.7a. The electron temperature is approximately 300 eV at the q = 2 surface and the local electron density is approximately 1×10^{19} m^{-3}. These parameters lead to magnetic Reynolds number $S = 8.6 \times 10^6$ and resistive time $\tau_R = 0.18$ s. Plasma viscosity is assumed to be at the anomalous transport level $\mu_\perp = 0.5$ m^2 s^{-1}.

The initial frequency of the TM is set to be 4 kHz. The amplitude of the RRMP at its flattop is scanned to investigate the dependence of the plasma response on the RRMP amplitude, while the dependence of the plasma response on the phase of locked TM is obtained by locking the TM to a 50 Hz slowly rotating RMP instead of a static RMP. In the results shown in this section, the RMP amplitude $\psi_{2/1}(r=a)$, W_{TM}, $b_\theta^{2/1}$ and T_e are normalized to aB_t, a, B_t and $T_e(r=0)$ respectively.

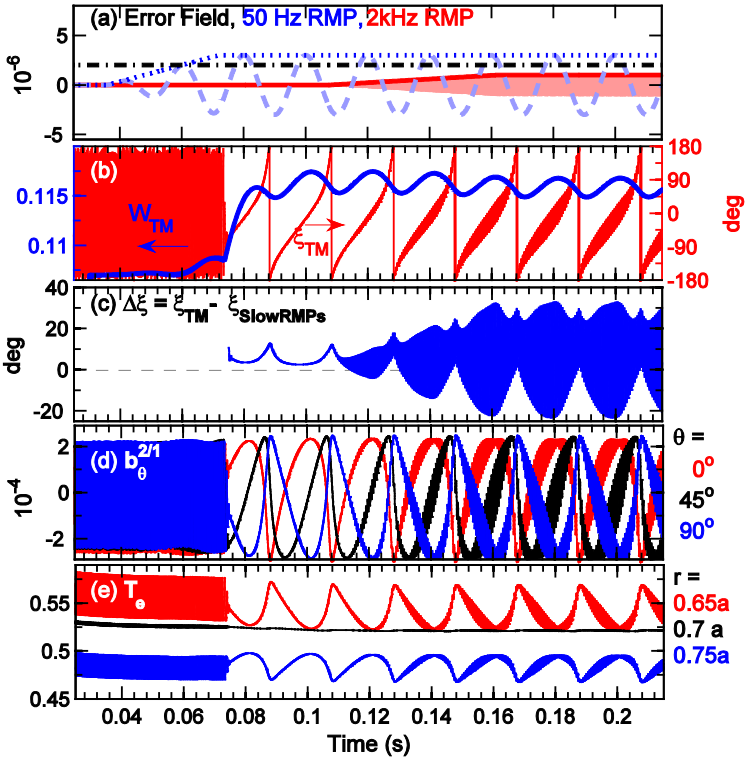

the application of slow RMPs (error field and 50 Hz RMP) and 2 kHz RRMP, modeled by TM1. (*a*) the error field, 50 Hz RMP, 2 kHz RMP, represented by $\psi_{2/1}(r = a)/(aB_t)$. (*b*) the island width (W_{TM}) and phase (ξ_{TM}). (*c*) the phase difference between TM and slow RMPs. (*d*) the perturbed m/n = 2/1 poloidal magnetic field, $b_\theta^{2/1}$, calculated at r/a = 0.85 and θ = 0°, 45°, 90°. (*e*) the electron temperature, T_e, calculated at θ = 0° and r/a = 0.65, 0.7 and 0.75. W_{TM}, $b_\theta^{2/1}$ and T_e are normalized to a, B_t and $T_e(r=0)$ respectively.

Fig. 11 Overview of the evolution of plasma parameters during

Fig. 11 displays one example of the numerical results. A 50 Hz rotating RMP is applied from 0.036 s and ramped up to 3×10^{-6}, while a static error field is applied at the amplitude of 2×10^{-6} from the beginning, as shown in Fig. 11(*a*). The sum of the 50 Hz RMP and the error field is termed as the "slow RMPs". The TM is locked to the slow RMPs at around 0.075s as indicated by the evolution of

TM phase (ξ_{TM}) in Fig. 11(*b*). After the locking of TM, the island width increases (Fig. 11 (*b*)) and the phase lag between TM and slow RMPs ($\Delta\xi = \xi_{TM} - \xi_{\text{slow RMPs}}$) is around $3^o \sim 15^o$ (Fig. 11 (*c*)).

To probe the plasma response, a fast rotating RMP at the frequency of 2 kHz is applied with a flattop of 1×10^{-6} when the 50 Hz locked TM reaches its steady state. Once the 2 kHz RRMP is applied, ξ_{TM} is significantly modulated, which can be clearly observed from $\Delta\xi$ (Fig. 11 (*c*)). $b_\theta^{2/1}$ is also affected, while those T_e signals obtained near 2/1 RS show similar features as the experimental results described previously in Fig. 4.

An expanded view of the plasma responses is shown in Fig. 12 during the flattop of the 2 kHz RRMP. Clear oscillations at 2 kHz could be observed from ξ_{TM} (Fig. 12(*a*)). The 2 kHz oscillation of island width is quite small, so it is not shown here. The plasma response to RRMP at f_{RRMP} = 2 kHz could be also clearly observed from $b_\theta^{2/1}$ (Fig. 12 (*c*)) and T_e (Fig. 12 (*e*)). The 2 kHz perturbation of $b_\theta^{2/1}(\theta=0^o)$ is always out of phase with that of $b_\theta^{2/1}(\theta=90^o)$, while the phase between $b_\theta^{2/1}(\theta=0^o)$ and $b_\theta^{2/1}(\theta=45^o)$ can be either in phase (0.195 – 0.2 s) or out of phase (0.202 – 0.206 s). The phase relations between different channels are consistent with the experimental observation, since the channels at $\theta = 0^o$ and 90^o are always at different sides of the O-/X-point for an m = 2 TM and the channels at $\theta = 0^o$ and 45^o are in the same (or different) side of the O-point of TM before (or after) 0.2 s. Besides, clear $2f_{RRMP}$ component can be observed from $b_\theta^{2/1}$ when it reaches its maximum or minimum. The poloidal distribution of $b_\theta^{2/1}$ (Fig. 12 (*d*)) shows that the location of maximal $b_\theta^{2/1}$ is oscillating around the averaged TM phase. The T_e perturbation at 2 kHz is also reversed between the channel inside (r/a = 0.65) and outside (r/a = 0.75) the 2/1 RS, and the amplitude of the T_e perturbation is minimal (maximinal) around O-/X- point (between O-/X- point) of TM. The phase of T_e response is in phase for channels at the same side of RS, as shown in Fig. 12 (*f*).

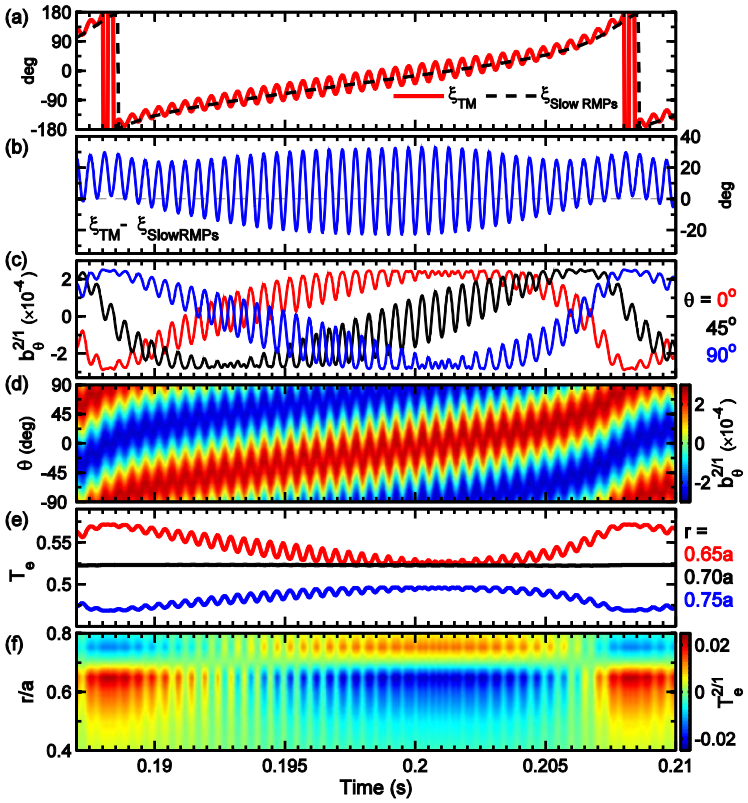

Fig. 12 Expanded view of the plasma responses to 2 kHz RRMP during its flattop. (*a*) the phase of TM (ξ_{TM}, red solid line) and the phase of the slow RMPs ($\xi_{SlowRMPs}$, black dashed line), (*b*) the phase difference between TM and slow RMPs, (*c*) $b_\theta^{2/1}$ calculated at r/a = 0.85 and θ = 0°, 45°, 90°. (*d*) poloidal distribution of $b_\theta^{2/1}$. (*e*) T_e calculated at θ = 0° and r/a = 0.65, 0.7 and 0.75. (*f*) the evolution of the radial distribution of $T_e^{2/1}$.

The amplitude and phase of the ξ_{TM} oscillation, $\delta\xi_{TM}(f_{RRMP})$ and $\phi_{TM}(f_{RRMP})$, are defined by $\xi_{TM} = \xi_{TM}^{ave} + \delta\xi_{TM}(f_{RRMP})\times\sin[2\pi f_{RRMP}t + \phi_{TM}(f_{RRMP})]$ for a sets of time durations of $2/f_{RRMP}$, where ξ_{TM}^{ave} the averaged TM phase. The phase and amplitude of $b_\theta^{2/1}$ and T_e perturbations ($\delta b_\theta^{2/1}$, $\phi_{b\theta}$, δT_e and ϕ_{Te}) are defined similarly, which has also been described in the end of Section 2.

The oscillation amplitude of ξ_{TM}, $\delta\xi_{TM}(f_{RRMP})$, is not constant during the flattop of RRMP, as shown in Fig. 12 (*b*). Fig. 13 shows the dependence of $\delta\xi_{TM}(f_{RRMP})$ on ξ_{TM}^{ave}. The RRMP amplitude is scanned and indicated by the color code. $\delta\xi_{TM}(f_{RRMP})$ reaches its maximum (respectively minimum) when ξ_{TM}^{ave} is approximately equal to -15° (140° respectively). With the increase of RRMP amplitude, $\delta\xi_{TM}$ also increases. The inserted panel in the upper right of Fig. 13 shows a linear dependence between $\delta\xi_{TM}$ and the amplitude of RRMP, hence proving Eq. (9) numerically.

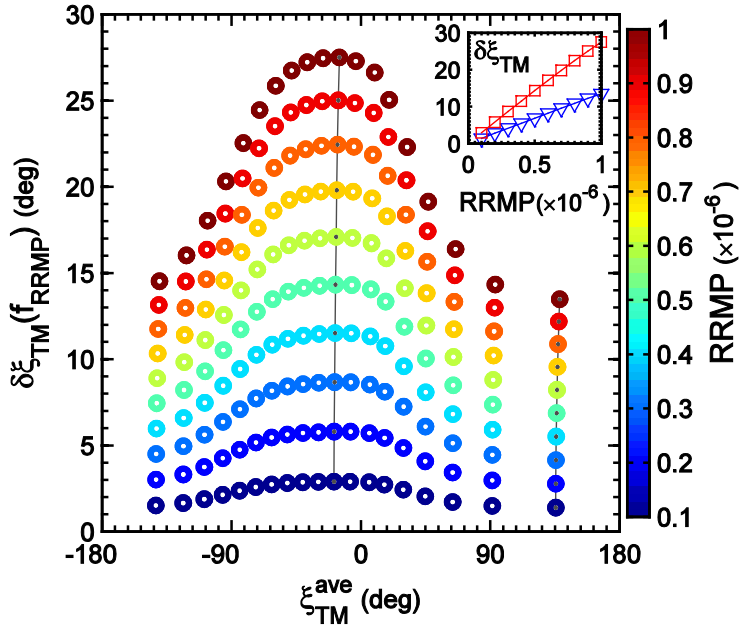

Fig. 13 The dependence of the oscillation amplitude of TM phase, $\delta\xi_{TM}(f_{RRMP})$, on the averaged TM phase, ξ_{TM}^{ave}, with the color code indicating the amplitude of RRMP. The inserted panel shows the dependence of the maximum (red squares) and minimum (blue triangles) of $\delta\xi_{TM}(f_{RRMP})$ at each RRMP amplitude on the amplitude of applied RRMP.

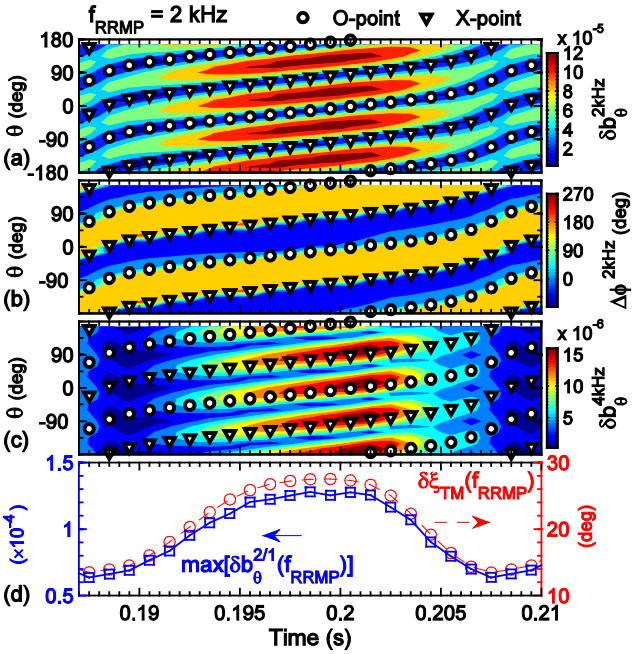

Fig. 14 The evolution of $b_\theta^{2/1}$ perturbation due to plasma response to 2 kHz RRMP with the 50 Hz rotation of TM. The time evolution of poloidal distribution of (*a*) amplitude and (*b*) relative phase (with respect to $\phi_{TM}(f_{RRMP})$) at fundamental frequency and (*c*) the amplitude at $2f_{RRMP}$ are shown. The rotation of TM is marked by the circles (O-points) and triangles (X-points) from (*a*) to (*c*). The time evolution of the maximal $b_\theta^{2/1}$ perturbation ($\max[\delta b_\theta^{2/1}(f_{RRMP})]$, blue squares) and $\delta\xi_{TM}(f_{RRMP})$ (red circles) are also shown in (*d*).

Fig. 14 displays the time evolution of the amplitude and phase of $b_\theta^{2/1}$ perturbations for the case shown in Fig. 12. As shown in Fig. 14(*a*), the amplitudes of $b_\theta^{2/1}$ perturbations at 2 kHz, δb_θ^{2kHz}, have four peaks poloidally, while their minima locate at the O- and the X-points of the TM. The relative phase between the TM phase oscillation and $b_\theta^{2/1}$ perturbation, $\Delta\phi^{2kHz} = \phi_{b\theta}(f_{RRMP}) - \phi_{TM}(f_{RRMP})$, is either around 0^o or 180^o, indicating that the $b_\theta^{2/1}$ perturbation is in (out of) phase with the phase oscillation of TM when $\partial b_\theta^{2/1}/\partial\xi<0$ (>0). The second harmonic of the $b_\theta^{2/1}$ perturbation, δb_θ^{4kHz}, has maxima at the O-/X-points of TM as shown in Fig. 14 (*c*). The poloidal maximum of $b_\theta^{2/1}$ perturbations ($\max[\delta b_\theta^{2/1}(f_{RRMP})]$, blue squares) evolves in a similar way as that of $\delta\xi_{TM}(f_{RRMP})$ (red circles), as shown in Fig. 14(*d*).

Since $\delta\xi_{TM}(f_{RRMP})$ has been observed at plenty of values in the modeling with the scan of RRMP

amplitude and the rotation of TM as shown in Fig. 13, a detailed relationship between max[$\delta b_\theta^{2/1}(f_{RRMP})$] and $\delta\xi_{TM}(f_{RRMP})$ could be obtained as shown in Fig. 15. The relationship is in good agreement with the sine function which is shown by the blue solid line. It has to be noted that the amplitude of the sine function (i.e. 2.7) is selected to be the amplitude of total $b_\theta^{2/1}$ which has been shown in Fig. 12(*c*). Both the dependence and parameter of this relationship have already been predicted by the phenomenological model as shown in Eq. (8) in Section 4.

The tangent line of the sine curve at the origin (black dashed line) can describe the relationship between max[$\delta b_\theta^{2/1}(f_{RRMP})$] and $\delta\xi_{TM}(f_{RRMP})$ very well at small oscillation amplitude, e.g. when $\delta\xi_{TM}(f_{RRMP}) < 25^o$. Since $\delta\xi_{TM}(f_{RRMP})$ is linear to the amplitude of RRMP (Fig. 13), the amplitude of magnetic perturbation, max[$\delta b_\theta^{2/1}(f_{RRMP})$], will be linear to the amplitude of RRMP. This is consistent with the experimental observation shown in Fig. 9 (*a*).

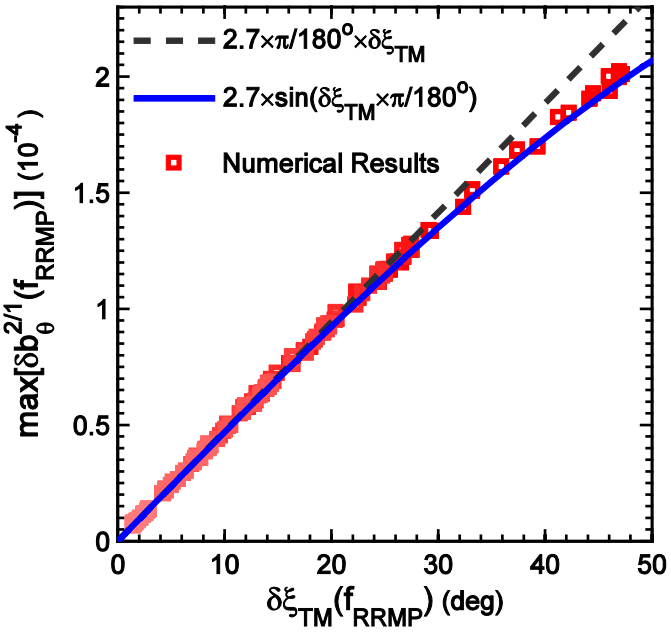

Fig. 15 The dependence of the poloidal maximum of $b_\theta^{2/1}$ perturbation, max[$\delta b_\theta^{2/1}(f_{RRMP})$], on the oscillation of TM phase, $\delta\xi_{TM}(f_{RRMP})$. The blue solid and black dashed lines show a sine curve and a linear line with the parameter 2.7 equaling to the amplitude of total $b_\theta^{2/1}$.

Fig. 16 displays the plasma response to RRMP, indicated by the T_e perturbations, as a function of the TM locations, ξ_{TM}^{ave}. The T_e signals are calculated at $\xi_{Te} = 0^o$ and various radial locations. Each point in Fig. 16(*a*, *b*, *c*, *e*) is calculated for a time duration of $2/f_{RRMP}$. With the rotation of TM at a period of 20ms, ξ_{TM}^{ave} varies from 0^o to 360^o, and hence $T_e(\xi=0^o)$ measures the O-point (or X-point) when $\xi_{TM}^{ave} = 0^o$ (or 180^o). In Fig. 16(*a*), the radial profile of $T_e^{ave}(r, \xi=0^o)$ is flattened at the O-point and with a large radial gradient at the X-point. At the O-/X-points, the poloidal T_e gradient is zero as shown in Fig. 16(*d*), since T_e is minimal or maximal poloidally. Fig. 16(*b*) shows the relative phase between the TM phase oscillation and T_e perturbation at f_{RRMP}, $\Delta\phi_{Te}^{2kHz} = \phi_{Te}(f_{RRMP}) - \phi_{TM}(f_{RRMP})$. It is found that $\Delta\phi_{Te}^{2kHz} = 0^o$ for $r = 0.6a$, $0.65a$ if $\xi_{TM}^{ave} \in [0^o, 180^o]$, and $r = 0.75a$, $0.8a$ if $\xi_{TM}^{ave} \in [180^o,$

360°]. Hence the T_e perturbations are in phase with the TM phase oscillations in these cases, where the local poloidal gradient of T_e, $\partial T_e/\partial\xi|_{\xi=0}$, is negative (Fig. 16(*d*)). For r =0.75*a*, 0.8*a* with $\xi_{TM}^{ave} \in [0^o, 180^o]$, or r = 0.6*a*, 0.65*a* with $\xi_{TM}^{ave} \in [180^o, 360^o]$, $\Delta\phi_{Te}^{2kHz} = 180^o$ and $\partial T_e/\partial\xi|_{\xi=0} > 0$. These observations are consistent with the sign of Eq. (11).

The amplitude of the T_e perturbation, $\delta T_e(f_{RRMP})$, is shown in Fig. 16(*c*), and its sign is set to be positive (respectively negative) when the response is in phase (out of phase respectively) with the TM phase oscillation. The dependence of $\delta T_e(f_{RRMP})$ on ξ_{TM}^{ave} is similar to that of $\partial T_e/\partial\xi|_{\xi=0}$. But $\delta T_e(f_{RRMP})$ at $\xi_{TM}^{ave} \sim 270^o$ is much larger than that of $\xi_{TM}^{ave} \sim 90^o$, while $\partial T_e/\partial\xi|_{\xi=0}$ has the same absolute value at these two TM locations. This can be explained by the relationship that $\delta T_e = -\partial T_e/\partial\xi \times \delta\xi_{TM}$ as described in Eq. (11) and the fact that $\delta\xi_{TM}(f_{RRMP})$ is larger at 270° than 90° as shown in Fig. 16(*e*). Fig. 17 confirms this explanation.

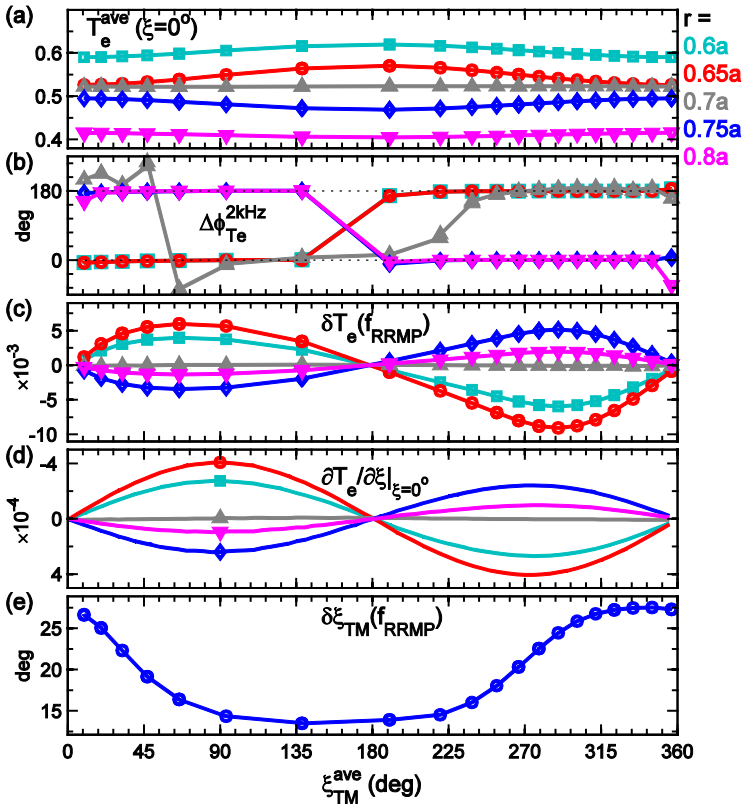

Fig. 16 The dependence of plasma response measured by T_e perturbation on ξ_{TM}^{ave} for the case shown in Fig. 12. (*a*) the averaged T_e, T_e^{ave}, (*b*) the phase difference between T_e perturbation and TM phase oscillation, $\Delta\phi_{Te}^{2kHz} = \phi_{Te}(f_{RRMP}) - \phi_{TM}(f_{RRMP})$, (*c*) the amplitude of T_e perturbation, $\delta T_e(f_{RRMP})$, (*d*) the poloidal gradient of T_e, $\partial T_e/\partial\xi|_{\xi=0}$ (the vertical-axis is reversed for the convenience of comparison), (*e*) the oscillation amplitude of TM phase, $\delta\xi_{TM}$. Each point in (*a*, *b*, *c*, *e*) is calculated for a time duration of $2/f_{RRMP}$. T_e is obtained at $\xi = 0^o$.

The detailed dependence of δT_e on $\delta\xi_{TM}$ is shown in Fig. 17 (*a*) for $\xi_{TM}^{ave} = 90^o$ (blue open symbols) and 270° (red filled symbols). The variation of $\delta\xi_{TM}$ is obtained by the scan of RRMP amplitude. The gray lines show a linear dependence on $\delta\xi_{TM}$ with the slope of $-\partial T_e/\partial\xi$ at these five radial locations. Since $-\partial T_e/\partial\xi$ has the same absolute value but different sign for $\xi_{TM}^{ave} = 90^o$ and 270° and the y-axis direction for the 270° case is reversed, these gray lines can represent for both $\xi_{TM}^{ave} = 90^o$ and 270°. It is found that $\delta T_e(f_{RRMP})$ is linear to $\delta\xi_{TM}(f_{RRMP})$ and the ratio corresponds to $-\partial T_e/\partial\xi$. To identify whether it is true for any ξ_{TM}^{ave}, the ratios between the amplitudes of T_e perturbation and

TM phase oscillation, $\delta T_e(f_{RRMP})/\delta\xi_{TM}$, are plotted as a function of ξ_{TM}^{ave} in Fig. 17(*b*) for $\delta\xi_{TM}$ between 5° and 20°. It is found that $\delta T_e/\delta\xi_{TM} = -\partial T_e/\partial\xi$ for all ξ_{TM}^{ave}, as predicted precisely by Eq. (11). In conclusion, the modelling results are consistent with the forced phase oscillation model that the measured plasma response is mainly due to the poloidal gradient of the plasma parameters combined with the phase oscillation of TM.

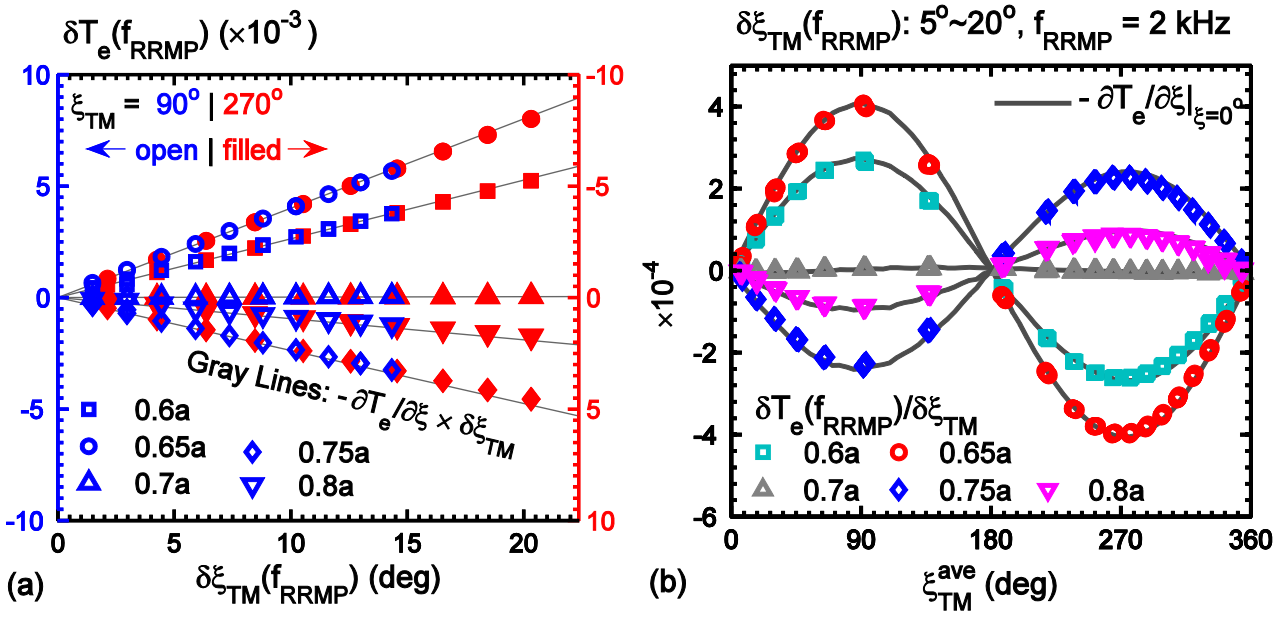

Fig. 17 (*a*) The dependence of $\delta T_e(f_{RRMP})$ on $\delta\xi_{TM}(f_{RRMP})$ for cases with f_{RRMP} = 2 kHz. Blue open (respectively red filled) symbols are obtained when ξ_{TM} = 90° (270° respectively). (*b*) The dependence of $\delta T_e(f_{RRMP})/\delta\xi_{TM}$ (open symbols) and $-\partial T_e/\partial\xi$ (gray lines) on the TM phase.

6. Summary and Discussion

6.1 Summary

We would like to summarize the main results of this paper as follows.

By using the rotating RMPs with a large 2/1 component, the plasma response to RRMP has been studied systematically in the presence of a locked 2/1 TM in the J-TEXT tokamak both experimentally and numerically. In the J-TEXT discharges without TMs, the plasma response to a rotating RMP showed a feature of travelling wave. After applying the RRMP field to the plasmas with a QSM/LM, the plasma responses to RRMP were measured with the following features:

(1) The magnetic perturbations had a *standing wave like* structure in the TM rest frame, including:

a) Four and two *nodes* of the response can be observed poloidally and toroidally, respectively. They were located around the O-/X- points of the 2/1 TM. The magnetic perturbation

measured near the *node* had a large $\delta b_\theta(2f_{RRMP})$ component, while the $\delta b_\theta(f_{RRMP})$ component was almost zero.

b) The magnetic perturbation measured at two channels between two adjacent *nodes* were in phase, but their phases were reversed between two channels on different side of a *node*.

(2) The T_e perturbation were zero or minimal inside the locked island or outside the magnetic island but at the same poloidal positions as the O-/X- points. The phases of the T_e perturbation are opposite between channels inside and outside the 2/1 RS.

(3) Both the T_e and b_θ perturbations increased linearly with the RRMP field.

A phenomenological model is proposed, showing that the TM phase is forced to oscillate due to the periodical EM torque applied by the RRMP. And the standing wave like features could be explained to be due to the combination of the forced phase oscillation of the TM and the poloidal gradient of those non-axisymmetric plasma parameters. The nonlinear numerical modeling results, based on reduced MHD equations, produce all the experimentally observed features of plasma response. The phase oscillation of the TM is observed, and the phase oscillation amplitude $\delta\xi_{TM}$ is shown to increase linearly with the increase of RRMP at small or moderate RRMP amplitude. The b_θ and T_e perturbations are shown to be proportional to the product of $\delta\xi_{TM}$ and the poloidal gradient of $b_\theta^{2/1}$ or T_e, respectively. These relationships demonstrate those predictions or assumptions which are made in the model of the forced phase oscillation of TM.

As a conclusion, the forced phase oscillation of the locked TM by RRMP has been observed experimentally and confirmed by the model and the numerical results. In the presence of a locked TM, the plasma response to RRMP is mainly due to the forced phase oscillation of TM and the poloidal gradient of plasma parameters.

6.2 Discussion on the experimental results

There are still some experimental observations which need to be discussed, although the qualitative agreements have been obtained between experiments and modelling.

The phase differences between the plasma response and the RRMP [$\Delta\phi(f_{RRMP}) = \phi_{b\theta}(f_{RRMP}) - \delta_4$, Fig. 7(*b*)] can't match between #1032192 and #1032502 after shifting the former one by $\Delta\theta_{LM} = +67.5^o$ poloidally, where 67.5^o is the poloidal separation of the locked TM between these two discharges. In the modelling, the experimental δ_4 can be represented by the phase of the real (or imaginary) part of RRMP, $\phi_{Re}(f_{RRMP})$, hence $\Delta\phi = \phi_{b\theta} - \phi_{Re} = [\phi_{b\theta} - \phi_{TM}] + [\phi_{TM} - \phi_{Re}]$. We then define $\Delta\phi = \Delta\phi_a + \Delta\phi_b$ with *a*) $\Delta\phi_a = \phi_{b\theta} - \phi_{TM}$, the phase difference between the plasma response and the

TM phase oscillation and *b*) $\Delta\phi_b = \phi_{TM} - \phi_{Re}$, the phase difference between the TM phase oscillation and the real part of RRMP. $\Delta\phi_a$ is either 0^o or 180^o, depending on the sign of the local poloidal gradient of $b_\theta^{2/1}$ and T_e (Fig. 10, Fig. 14(*b*) and Fig. 16(*b*)). Hence $\Delta\phi_a$ will determine the waveform of the poloidal distribution of $\Delta\phi$, especially, the locations of the phase jump which coincide with the O- and X- points of the TM. $\Delta\phi_b$ is the same for all poloidal and toroidal locations, hence it determines the vertical shift of the poloidal distribution of $\Delta\phi$. ϕ_{Re} is defined by describing the real part of RRMP as $b_{RRMP}^{Re} = b_{RRMP}\times\sin[2\pi f_{RRMP}t + \phi_{Re}(f_{RRMP})]$. Note that $b_{RRMP}^{Re} = b_{RRMP}\times\sin[\xi_{RRMP}(t) + 90^o]$, hence $\phi_{Re}(f_{RRMP}) = \xi_{RRMP}(t) + 90^o - 2\pi f_{RRMP}t = \xi_{RRMP}(t_0) + 90^o$, where t_0 is the beginning of those sets of time durations used for calculating $\phi_{TM}(f_{RRMP})$. Fig. 18 displays the dependence of $\Delta\phi_b$ on ξ_{TM}^{ave} for the case shown in Fig. 12. It is clearly shown that $\Delta\phi_b$ varies significantly with ξ_{TM}^{ave}. The LM phases of the two cases compared in Fig. 7(*b*) have a difference of $\Delta\xi_{LM} = 2\Delta\theta_{LM} = 135^o$, which contributes to a large difference of $\Delta\phi_b$ and hence leads to the observation that $\Delta\phi$ couldn't match between these two discharges after shifting the waveform by $\Delta\theta_{LM}$.

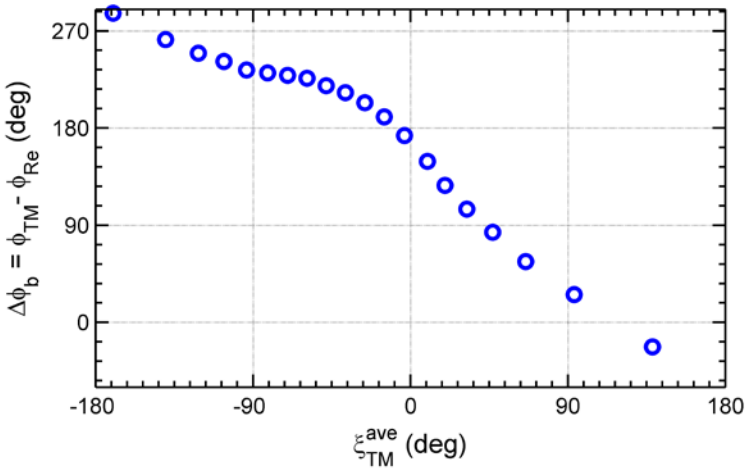

Fig. 18 The dependence of the phase difference between the TM phase oscillation and the real part of RRMP, $\Delta\phi_b = \phi_{TM} - \phi_{Re}$, on the averaged TM phase, ξ_{TM}^{ave}, for the case shown in Fig. 12.

It is still unclear why the plasma response measured by b_θ perturbation in case 1 was larger than that of case 2 (Fig. 9 (*a*)). According to Eq. (8) and the modelling result shown in Fig. 15, $\delta b_\theta^{max} = b_\theta^{2/1}(\xi_{O\text{-point}})\times\delta\xi_{TM}$, with $b_\theta^{2/1}(\xi_{O\text{-point}})$ the $b_\theta^{2/1}$ at the O-point. The locked TMs in case 1 were smaller than that of case 2, hence $b_\theta^{2/1}(\xi_{O\text{-point}})$ was smaller in case 1. $\delta\xi_{TM}$ could be affected by the slow RMPs, the RRMP, the island width and the island phase, so it is very complicated. Fig. 13 shows numerically that $\delta\xi_{TM}$ varies at different TM phases while keeping the RRMP constant. If $\delta\xi_{TM}$ were much larger in case 1 than in case 2, the b_θ perturbation could be larger in case 1. Since $\delta\xi_{TM}$ couldn't be measured experimentally yet, this assumption remains to be demonstrated in the future.

The locked TMs were maintained at small sizes to avoid disruptions, and no minor disruptions were observed in the discharges related to this paper. Hence the width of the locked TM might not be

large enough to induce secondary structures as predicted by the theory [55]. Besides, the spatial resolution of the ECE measurement in J-TEXT is not high enough to identify the possible appearance of the secondary structures [34]. The attempt to observe the secondary structure will only be possible with the ECEI system [56] and a larger island. Hence it is supposed that the standing wave like plasma response should not be related to the secondary structures.

6.3 Discussion on possible applications

This paper provides a further validation of the present theory. Almost all of the experimental features of the standing wave like plasma response, which have not been described before, are reproduced by the nonlinear numerical modelling and the phenomenological model. These results advance the understanding in the unlocking process of the LM by RRMP in J-TEXT [35]. It is shown that $\delta\xi_{\mathrm{TM}}$ increases with the RRMP. Further increasing the RRMP amplitude in the modelling, $\delta\xi_{\mathrm{TM}}$ exceeds a critical value, then the TM is unlocked from the slow RMPs and is locked to the RRMP. To improve the efficiency of unlocking the LM by using RRMP, it will be necessary to investigate how to increase $\delta\xi_{\mathrm{TM}}$ both numerically and experimentally. Further study is still needed for predicting the thresholds of LM unlocking, in order to avoid the LM disruption for a fusion reactor.

This work provides an alternative method, as a supplement to LMDs, to identify the presence of a locked island and to measure the internal properties of this locked island. It is challenging to identify the formation of a small locked island, e.g. the locked island induced at the pedestal top which is proposed to explain the ELM suppression by external MP field in DIII-D [57]. The non-axisymmetric b_{r} measured by LMD could be due to either the formation of a small locked island or other kinds of plasma responses, e.g. resonant field amplification (RFA) [58, 59], kink mode [60], kink-ballooning or kink-peeling modes [61], etc. By superimposing a small fast rotating RMP field on the flattop of the static RMP field, the phase of the locked island could be forced to oscillate if it does exist. This would lead to a standing wave like feature of the magnetic perturbations which could be easily measured by Mirnov probes, and perhaps even from the T_{e} and n_{e} measurements. This unique feature is a direct evidence that a locked island exists.

Acknowledgments

The authors are grateful to Dr. Yunfeng Liang for helpful discussions and to the referees for fruitful suggestions. This work is supported by National Magnetic Confinement Fusion Science

Program of China (Contract No. 2014GB118000, 2015GB111001 and 2013GB106003B), the National Natural Science Foundation of China (Contract No. 11275080, 11405068 and 11505069) and the Initiative Postdocs Supporting Program of China (Grant No. BX201700090). N.W. is thankful for the support from the China Scholarship Council.

References

[1] Igochine V (ed.), 2015 Active Control of Magneto-hydrodynamic Instabilities in Hot Plasmas, *Springer Series on Atomic, Optical, and Plasma Physics* **83**

[2] Evans T E *et al* 2015 Resonant magnetic perturbations of edge-plasmas in toroidal confinement devices *Plasma Phys. Control. Fusion* **57** 123001

[3] Morris A W *et al* 1990 Feedback Stabilization of Disruption Precursors in a Tokamak *Phys. Rev. Lett.* **64** 1254

[4] Hender T C *et al* 1992 Effect of resonant magnetic perturbations on COMPASS-C tokamak discharges *Nucl. Fusion* **32** 2091

[5] Fitzpatrick R *et al* 1993 Interaction of tearing modes with external structures in cylindrical geometry (plasma) *Nucl. Fusion* **33** 1049

[6] Hu Q *et al* 2013 Understanding the effect of resonant magnetic perturbations on tearing mode dynamics *Phys. Plasmas* **20** 092502

[7] Waelbroeck F L 2009 Theory and observations of magnetic islands *Nucl. Fusion* **49** 104025

[8] Garofalo A M *et al* 1999 Stabilization of the external kink and control of the resistive wall mode in tokamaks *Phys. Plasmas* **6** 1893

[9] Chu M S and Okabayashi M 2010 Stabilization of the external kink and the resistive wall mode *Plasma Phys. Control. Fusion* **52** 123001

[10] Evans T E *et al* 2004 Suppression of Large Edge-Localized Modes in High-Confinement DIII-D Plasmas with a Stochastic Magnetic Boundary *Phys. Rev. Lett.* **92** 235003

[11] Liang Y *et al* 2007 Active Control of Type-I Edge-Localized Modes with n = 1 Perturbation Fields in the JET Tokamak *Phys. Rev. Lett.* **98** 265004

[12] Fitzpatrick R and Hender T C 1991 The interaction of resonant magnetic perturbations with rotating plasmas *Phys. Fluids* B **3** 644–73

[13] Waelbroeck F L 2012 Role of singular layers in the plasma response to resonant magnetic perturbations *Nucl. Fusion* **52** 074004

[14] Narushima Y *et al* 2017 Observations of sustained phase shifted magnetic islands from externally imposed $m/n = 1/1$ RMP in LHD *Nucl. Fusion* **57** 076024

[15] Denner P *et al* 2014 Local measurements of screening currents driven by applied RMPs on TEXTOR *Nucl. Fusion* **54** 064003

[16]Ryan D A *et al* 2015 Toroidal modelling of resonant magnetic perturbations response in ASDEX-Upgrade: coupling between field pitch aligned response and kink amplification *Plasma Phys. Control. Fusion* **57** 095008

[17] Orain F *et al* 2017 Non-linear modeling of the plasma response to RMPs in ASDEX Upgrade *Nucl. Fusion* **57** 022013

[18] Wang H H *et al* 2016 Observation of spectrum effect on the measurement of intrinsic error field on EAST *Nucl. Fusion* **56** 066011

[19] Kirk A *et al* 2015 Effect of resonant magnetic perturbations on low collisionality discharges in MAST

and a comparison with ASDEX Upgrade *Nucl. Fusion* **55** 043011
[20] Paz-Soldan C *et al* 2015 Observation of a Multimode Plasma Response and its Relationship to Density Pump out and Edge-Localized Mode Suppression *Phys. Rev. Lett.* **114** 105001
[21] Shiraki D *et al* 2013 Measurement of 3D plasma response to external magnetic perturbations in the presence of a rotating external kink *Phys. Plasmas* **20** 102503
[22] Bolzonella T *et al* 2008 Resistive-Wall-Mode Active Rotation in the RFX-Mod Device *Phys. Rev. Lett.* **101** 165003
[23] Igochine V *et al* 2009 Externally induced rotation of the resistive wall modes in RFX-mod *Plasma Phys. Control. Fusion* **51** 055008
[24] Rao B *et al* 2013 First observation of rotation acceleration of magnetic island by using rotating resonant magnetic perturbation on the J-TEXT tokamak *Plasma Phys. Control. Fusion* **55** 122001
[25] Fietz S *et al* 2015 Influence of externally applied magnetic perturbations on neoclassical tearing modes at ASDEX Upgrade *Nucl. Fusion* **55** 013018
[26] Fridström R *et al* 2015 Hysteresis in the tearing mode locking/unlocking due to resonant magnetic perturbations in EXTRAP T2R *Plasma Phys. Control. Fusion* **57** 104008
[27] Rao B *et al* 2013 Tearing mode suppression by using resonant magnetic perturbation coils on J-TEXT tokamak *Phys. Lett. A* **377** 315
[28] Elgriw S *et al* 2011 Control of magnetic islands in the STOR-M tokamak using resonant helical fields *Nucl. Fusion* **51** 113008
[29] Yu Q and Günter S 2008 Locking of neoclassical tearing modes by error fields and its stabilization by RF current *Nucl. Fusion* **48** 065004
[30] La Haye R J *et al* 2006 Cross–machine benchmarking for ITER of neoclassical tearing mode stabilization by electron cyclotron current drive *Nucl. Fusion* **46** 451
[31] Buttery R J *et al* 2012 The limits and challenges of error field correction for ITER *Phys. Plasmas* **19** 056111
[32] Volpe F A *et al* 2009 Advanced techniques for neoclassical tearing mode control in DIII-D *Phys. Plasmas* **16** 102502
[33] Volpe F A *et al* 2015 Avoiding Tokamak Disruptions by Applying Static Magnetic Fields That Align Locked Modes with Stabilizing Wave-Driven Currents *Phys. Rev. Lett.* **115** 175002
[34] Liang Y *et al* 2007 Observations of secondary structures after collapse events occurring at the q = 2 magnetic surface in the TEXTOR tokamak *Nucl. Fusion* **47** L21
[35] Jin H *et al* 2015 Locked mode unlocking by rotating resonant magnetic perturbations in J-TEXT tokamak *Plasma Phys. Control. Fusion* **57** 104007
[36] Olofsson K E J *et al* 2016 Electromechanical modelling and design for phase control of locked modes in the DIII-D tokamak *Plasma Phys. Control. Fusion* **58** 045008
[37] Okabayashi M *et al* 2017 Avoidance of tearing mode locking with electro-magnetic torque introduced by feedback-based mode rotation control in DIII-D and RFX-mod *Nucl. Fusion* **57** 016035
[38] Inoue S *et al* 2018 Dependence of locked mode behavior on frequency and polarity of a rotating external magnetic perturbation *Plasma Phys. Control. Fusion* **60** 025003
[39] Zhuang G *et al* 2011 The reconstruction and research progress of the TEXT-U tokamak in China *Nucl. Fusion* **51** 094020
[40] Rao B *et al* 2014 Introduction to resonant magnetic perturbation coils of the J-TEXT tokamak *Fusion Eng. Des.* **89** 378
[41] Rao B *et al* 2012 *IEEE Trans. Appl. Supercond.* **22** 4201804
[42] Yi B *et al* 2013 Design of the power system for dynamic resonant magnetic perturbation coils on the

J-TEXT tokamak *Fusion Eng. Des.* **88** 1528
[43] Hu Q *et al* 2014 Influence of rotating resonant magnetic perturbations on particle confinement *Nucl. Fusion* **54** 122006
[44] Ding Y H *et al* 2014 Analytical compensation of axisymmetric equilibrium fluxes picked up by locked mode detectors in tokamaks *Rev. Sci. Instrum.* **85** 043502
[45] Yang Z J *et al* 2012 A 16-channel heterodyne electron cyclotron emission radiometer on J-TEXT *Rev. Sci. Instrum.* **83** 10E313
[46] Wang N *et al* 2014 Study of the penetration of resonant magnetic perturbations in J-TEXT *Nucl. Fusion* **54** 064014
[47] Wang H H *et al* 2018 Density scaling on $n = 1$ error field penetration in ohmically heated discharges in EAST *Nucl. Fusion* **58** 056024
[48] Hu Q *et al* 2016 Plasma response to $m/n = 3/1$ resonant magnetic perturbation at J-TEXT Tokamak *Nucl. Fusion* **56** 092009
[49] Rao B *et al* 2013 Measurement of 2/1 intrinsic error field of Joint TEXT tokamak *Rev. Sci. Instrum.* **84** 043504
[50] Fitzpatrick R 1995 Helical temperature perturbations associated with tearing modes in tokamak plasmas *Phys. Plasmas* **2** 825
[51] Yu Q *et al* 2004 Numerical modeling of nonlinear growth and saturation of neoclassical tearing modes *Phys. Plasmas* **11** 140
[52] Hu Q *et al* 2012 Effect of externally applied resonant magnetic perturbations on resistive tearing modes *Nucl. Fusion* **52** 083011
[53] Yu Q 2010 Linear and nonlinear stability of drift-tearing mode *Nucl. Fusion* **50** 025014
[54] Hu Q *et al* 2014 Enhanced particle transport caused by resonant magnetic perturbations in the J-TEXT tokamak *Nucl. Fusion* **54** 064013
[55] Loureiro N F *et al* 2015 X-Point Collapse and Saturation in the Nonlinear Tearing Mode Reconnection *Phys. Rev. Lett.* **95** 235003
[56] Pan X M *et al* 2016 Design of the 2D electron cyclotron emission imaging instrument for the J-TEXT tokamak *Rev. Sci. Instrum.* **87** 11E106
[57] Nazikian R *et al* 2015 Pedestal Bifurcation and Resonant Field Penetration at the Threshold of Edge-Localized Mode Suppression in the DIII-D Tokamak *Phys. Rev. Lett.* **114** 105002
[58] Garofalo A M *et al* 2003 Analysis of stable resistive wall modes in a rotating plasma *Phys.Plasmas* **10** 4776
[59]Gryaznevich M P *et al* 2008 Experimental studies of stability and beta limit in JET *Plasma Phys. Control. Fusion* **50** 124030
[60] King J D *et al* 2016 Landau resonant modification of multiple kink mode contributions to 3D tokamak equilibria *Nucl. Fusion* **56** 014003
[61] Paz-Soldan C *et al* 2016 Equilibrium drives of the low and high field side $n = 2$ plasma response and impact on global confinement *Nucl. Fusion* **56** 056001